


Quantitative analysis of the yeast pheromone pathway

James P. Shellhammer¹ | Amy E. Pomeroy²  | Yang Li³ | Lorena Dujmusic¹ | Timothy C. Elston^{1,2} | Nan Hao³ | Henrik G. Dohlman^{1,2}

¹Department of Pharmacology, University of North Carolina at Chapel Hill, Chapel Hill, NC 27599, USA

²Curriculum in Bioinformatics and Computational Biology, University of North Carolina at Chapel Hill, Chapel Hill, NC 27599, USA

³Division of Biological Sciences, University of California San Diego, San Diego, CA 92093, USA

Correspondence

Henrik G. Dohlman, University of North Carolina at Chapel Hill, Department of Pharmacology, Genetic Medicine Research Building, Suite 4016, Chapel Hill, NC 27599-7365, USA.

Email: henrik_dohlman@med.unc.edu; hdohlman@med.unc.edu

Present Address

James P. Shellhammer, Centre for Bionano Interactions, University College Dublin, Dublin, Ireland.

Funding information

NIH, Grant/Award Numbers: R01GM111458, R01GM114136 and R35GM118105

Abstract

The pheromone response pathway of the yeast *Saccharomyces cerevisiae* is a well-established model for the study of G proteins and mitogen-activated protein kinase (MAPK) cascades. Our longstanding ability to combine sophisticated genetic approaches with established functional assays has provided a thorough understanding of signalling mechanisms and regulation. In this report, we compare new and established methods used to quantify pheromone-dependent MAPK phosphorylation, transcriptional induction, mating morphogenesis, and gradient tracking. These include both single-cell and population-based assays of activity. We describe several technical advances, provide example data for benchmark mutants, highlight important differences between newer and established methodologies, and compare the advantages and disadvantages of each as applied to the yeast model. Quantitative measurements of pathway activity have been used to develop mathematical models and reveal new regulatory mechanisms in yeast. It is our expectation that experimental and computational approaches developed in yeast may eventually be adapted to human systems biology and pharmacology.

KEYWORDS

Saccharomyces cerevisiae, signal transduction, systems biology

1 | INTRODUCTION

G protein-coupled receptors (GPCRs) are conserved across biological kingdoms and respond to a variety of chemical and environmental signals. These signals are physicochemically diverse and include steroids, biogenic amines, polypeptides, ions, odours, tastes, and light. Generally speaking, these inputs lead to changes in second messenger and protein kinase activity, as well as new gene transcription and metabolic changes. A simple, yet powerful, model to study G protein signalling is the budding yeast *Saccharomyces cerevisiae*. Yeast use a GPCR to respond to peptide pheromones, which activate a G protein, mitogen-activated protein kinases (MAPKs), and transcription factors necessary for mating. Moreover, sophisticated genetic approaches in yeast have led to several important discoveries, including the first

ligand binding GPCR to be sequenced (Burkholder & Hartwell, 1985). Other landmarks include the first identification of a G protein GTPase activating protein (GAP) and the identification of a three-tiered MAPK cascade and MAPK scaffold (Reviewed in Alvaro & Thoner, 2016; Hao, Behar, Elston, & Dohlman, 2007). The pheromone response pathway has also been adapted for a variety of discovery applications. These include the systematic identification of ligands for human GPCRs expressed in yeast (Dowell & Brown, 2009; Minic, Sautel, Salesse, & Pajot-Augy, 2005; reviewed in Minic et al., 2005) and the directed evolution of designer GPCRs for chemogenetics applications (DREADDs; Dong, Rogan, & Roth, 2010; Pei, Dong, & Roth, 2010).

The pheromone signalling pathway in yeast initiates events necessary for the mating of haploid a and α cells. These haploid cell types secrete specific pheromones, a -factor and α -factor, that bind to cognate receptors on cells of the opposite type. Once activated, the receptors promote the exchange of GDP for GTP on the G protein α

James P. Shellhammer and Amy E. Pomeroy contributed equally to this work.

subunit (Gpa1) and dissociation of G α from the G $\beta\gamma$ subunit complex (Ste4/18). G $\beta\gamma$ then binds to (a) the adaptor protein Far1, (b) the p21-activated kinase Ste20, and (c) the kinase scaffold protein Ste5. Far1 recruits Cdc24, which activates the small G protein Cdc42 and promotes cell polarization toward the pheromone stimulus. Ste5 assembles and activates components of a kinase signalling cascade, which is in turn activated by Ste20. MAPK activation is required for multiple facets of the pheromone response including new gene transcription. Collectively, these events serve to prepare the cells for mating to form the α/α diploid (Erdman, Lin, Malczynski, & Snyder, 1998; Hagen, McCaffrey, & Sprague, 1991).

There are several features that have made yeast a particularly useful model for the study of GPCR signalling. First and foremost, the pheromone pathway shares extensive similarity to GPCR pathways in humans. Compared with most other eukaryotes however, the yeast pheromone pathway exists only in haploid cells and is composed of few functionally redundant isoforms. Moreover, yeast have the ability to undergo efficient homologous recombination. Thus, any given step of the pathway can be abrogated through deletion of a single gene. Finally, pathway output is easily determined through quantitative assays of MAPK activity and transcriptional induction. Collectively, these features have helped to establish the function of key pathway components *in vivo*.

More recently, yeast has served as a platform for systems biology applications, including the development of computational models that consider time- and stimulus-dependent changes in protein activity, localization, and expression. These efforts require quantitative measures of pathway activity, and in particular, how activity is affected by changes in the intensity or duration of the input stimulus. Such efforts can help to reveal how feedback inhibition—for example, desensitization to odours or drugs—confers such dramatic changes in GPCR signalling. Other forms of dynamic behaviour are important in gradient tracking—for example, to locate an invading pathogen or distant mating partner. Thus, any comprehensive understanding of signal transduction will require quantitative measures of activity, over time and in space, in a variety of genetic backgrounds.

Here, we describe newer quantitative measures of pheromone pathway activity. Our target audience is anyone interested in experimental approaches for yeast systems biology. We begin with a description of population-based assays and then consider several new single-cell approaches. We compare the advantages and disadvantages of each method, describe new technical improvements, discuss scenarios where each is favoured, and provide examples of how such methods have advanced our understanding of signal transduction in general. All of the assays are, in our experience, sufficiently robust and reliable for adoption in any well-equipped laboratory. To illustrate their ability to quantify differences in activity, we compare wild-type cells with mutants that exhibit elevated sensitivity to α -factor and sustained activation of the pathway. The strain BY4741 is used because most of the genes have been systematically deleted and fused to either green fluorescent protein (GFP) or a variety of affinity tags (Gelperin et al., 2005; Ghaemmaghami et al., 2003; Huh et al., 2003; Martzen et al., 1999; Winzeler et al., 1999), all at the native

locus and under the control of the native promoter. Thus, it is possible to simultaneously monitor pathway activity as well as the expression or localization of nearly every protein, in a variety of genetic backgrounds and under different experimental conditions. The two mutant strains provide a benchmark for comparing the methods. The first contains a G protein that is insensitive to the GTPase activating protein Sst2 (DiBello et al., 1998). The second lacks the secreted protease Bar1, which degrades α -factor pheromone (Ciejek & Thorner, 1979; MacKay et al., 1991). Both Sst2 and Bar1 are transcriptionally induced in response to pheromone and are consequently required for desensitization. Sst2 is also required for proper gradient tracking, whereas Bar1 is required for proper gradient formation (Andrews, Addy, Brent, & Arkin, 2010; Barkai, Rose, & Wingreen, 1998; Diener et al., 2014; Dixit, Kelley, Houser, Elston, & Dohlman, 2014; Jin et al., 2011; Kelley et al., 2015; Moore, Chou, Nie, Jeon, & Yi, 2008; Moore, Tanaka, Kim, Jeon, & Yi, 2013; Segall, 1993). Collectively, these mutants and measurements have helped to establish predictive models that are transforming our understanding of cell signal regulation.

2 | MATERIALS AND METHODS

2.1 | Strains and plasmids

All strains were generated from BY4741 ("wild-type"; Brachmann et al., 1998) and transformed by the lithium acetate method (Gietz & Woods, 2002). Replacement of *GPA1* with the GAP-insensitive mutant (*gpa1*^{G3025}) was done as previously described (Lambert et al., 2010). Genetic deletion of *BAR1* was achieved by homologous recombination of PCR-amplified G418 drug resistance gene from plasmid pFA6a-KanMX6 or the hygromycin B drug resistance gene from plasmid pFA6a-hphMX6 (Wach, Brachat, Pöhlmann, & Philippsen, 1994). *Kss1-9xMyc*-tagged strains were generated by homologous recombination of a PCR-amplified 9xMyc cassette harbouring a resistance gene to hygromycin B from plasmid pYM20 (pYM-9xMyc-hphNT1; Janke et al., 2004) at the C-terminus of the *KSS1* open reading frame (ORF). *Nhp6a-iRFP*-tagged strains were generated by homologous recombination of a PCR-amplified iRFP-*HIS3* cassette from plasmid pKT-iRFP-HIS (AkhavanAghdam, Sinha, Tabbaa, & Hao, 2016). The kinase translocation reporter (KTR) for Fus3 was integrated at the *TDH3* promoter following *SnaBI* digestion of plasmid pRS305 pTDH3-KTR (Li, Roberts, AkhavanAghdam, & Hao, 2017). *BEM1-GFP* was introduced by homologous recombination following PCR amplification of the *BEM1-GFP* ORF from the GFP-tagged library strain (Huh et al., 2003). GFP and mCherry reporters were introduced as described previously (Dixit et al., 2014). Briefly, the GFP reporter was integrated at the *FUS1* promoter following *XcmI* digestion of pRS303 *FUS1-GFP*. The mCherry reporter was integrated at the *ADH1* promoter following *PacI* digestion of *ADH1-mCherry* in pRS406 (WT and *bar1* Δ strain) or pRS405 (*gpa1*^{G3025} strain).

The pRS426-P_{FUS1}-YeGFP3 plasmid was generated by subcloning the YeGFP3 gene (Cormack et al., 1997) under control of the yeast *FUS1* promoter from plasmid pDS30 (Siekhaus & Drubin, 2003) into

plasmid pRS426 (Sikorski & Hieter, 1989) by digestion with *Bam*HI and *Xho*I, and subsequent ligation of gel-purified products. Plasmid pRS423-P_{FUS1}-LacZ was described previously (Hoffman, Garrison, & Dohlman, 2000) and is composed of a *Hind*III-*Hind*III restriction digest fragment containing the P_{FUS1}-LacZ sequence inserted at the *Hind*III site of plasmid pRS423.

2.2 | Sample preparation for Phospho-MAPK analysis

Cells were grown to saturation overnight in synthetic complete medium supplemented with antibiotics or lacking specific nutrients to maintain plasmid selection, and containing 2% wt/volume dextrose (hereafter, SCD medium or SCD - nutrient) at 30°C, diluted to OD₆₀₀ = 0.10, grown to OD₆₀₀ ~ 0.6–0.8, and then diluted again and grown to OD₆₀₀ ~ 1.0. A 3 mM stock of α -factor was then added to a final concentration of 3 μ M or 0.3 μ M. Aliquots were collected either before pheromone addition or after 5, 15, 30, 60, or 90 min, mixed with 6.1 N trichloroacetic acid (TCA) to 5% final concentration, and placed on ice. Cells were collected by centrifugation at 2,000 \times g for 2 min at 4°C, washed once with ice-cold 10 mM NaN₃, and re-collected by centrifugation at 16,000 \times g for 1 min. Cell pellets were stored at -80°C until use.

The same cell lysates were used for both conventional and Phos-tag SDS-PAGE and were prepared using conditions optimized for Phos-tag SDS-PAGE as described previously (English et al., 2015). Briefly, cell pellets were thawed on ice and resuspended in ice-cold TCA buffer (Lee & Dohlman, 2008) without EDTA (10 mM Tris-HCl, 10% TCA, 25 mM ammonium acetate, pH 8.0). Cells were vortexed for 10 min at 4°C and then collected by centrifugation at 16,000 \times g for 10 min at 4°C. Pellets were reconstituted in resuspension buffer (100 mM Tris-HCl, 3% sodium dodecyl sulphate [SDS], pH 11.0), heated at 99°C for 10 min, cooled to room temperature for 10 min, and centrifuged at 16,000 \times g for 1 min. Supernatants were then transferred to new tubes, and 5 μ l were used in a Bio-Rad DC Protein Assay (Bio-Rad #5000112) carried out according to the manufacturer's instructions. Absorbance values were compared against bovine serum albumin standards prepared in resuspension buffer. Lysates were normalized with resuspension buffer to 2 μ g/ μ l, mixed 1:1 with 2 \times SDS sample buffer (500 mM Tris-HCl, 20% (v/v) glycerol, 2% (w/v) SDS, 200 mM dithiothreitol, and 0.01% (w/v) bromophenol blue, pH 8.5) and used immediately or stored at -80°C. Samples were heated at 70°C for 10 min prior to loading.

2.3 | Conventional SDS-PAGE and immunoblotting

Thirty micrograms of protein sample were loaded onto 10% SDS-PAGE gels and run in SDS electrophoresis buffer (25 mM Tris base, 20 mM glycine, 0.1% [w/v] SDS, pH 8.3) at room temperature for 20 min at 20 mA/gel. After proteins transited the stacking layer, the current was increased to 25 mA/gel for 110 min. The resolving layer was removed, equilibrated in transfer buffer (20% methanol, 25 mM

Tris Base, 200 mM glycine), and then transferred to nitrocellulose membranes at 100 V for 90 min in transfer buffer at 4°C.

Nitrocellulose membranes were placed in an SDS-PAGE blocking buffer comprising TBS-T (100 mM Tris Base, 150 mM NaCl, 0.1% Tween-20, pH 7.5), 5% (w/v) non-fat dry milk, and 10 mM NaN₃, for 1 hr at room temperature, and then probed with antibodies to phospho-p44/42 (Cell Signalling #4370, 1:500 ratio), Fus3 (Santa Cruz Biotechnology #6773, 1:500 ratio), Myc (Kss1-Myc; Clone 9B11, Cell Signalling Technology #2276, 1:1,000 ratio), or glucose-6-phosphate dehydrogenase (G6PDH) as a loading control (Sigma #A9521, 1:50,000 ratio) for 1 hr at room temperature (G6PDH) or overnight at 4°C with shaking. Blots were washed 3 \times 5 min with TBS-T and then incubated with horseradish peroxidase-conjugated goat anti-rabbit (Bio-Rad #1662408), donkey anti-mouse (Jackson ImmunoResearch #715-035-151), or donkey anti-goat (Santa Cruz Biotechnology #sc-2020) secondary antibodies at 1:10,000 in TBS-T containing 5% (w/v) non-fat dry milk for 1 hr at room temperature. Blots were washed 3 \times 5 min with TBS-T and after a 5-min incubation with Clarity ECL Western Blotting Substrate (Bio-Rad # 1705061) imaged on a Bio-Rad ChemiDoc MP imaging system. Phospho-MAPK antibodies were removed by treatment with Stripping Buffer (62.5 mM Tris-HCl, 2% [w/v] SDS, 100 mM β -mercaptoethanol, pH 6.8) for 30 min in a dry oven at 65°C, with occasional agitation by hand, then rinsed thoroughly with distilled water and finally with TBS-T 3 \times 10 min before re-probing for total MAPK (combined anti-Fus3 and anti-Myc antibodies). Blots were stripped once again and re-probed for G6PDH as a loading control.

2.4 | Phos-tag SDS-PAGE and immunoblotting

Ten percent bis-tris SDS-PAGE gels containing 50 μ M Phos-tag (Wako) and 100 μ M Zn (NO₃)₂ were prepared as described previously (English et al., 2015). Briefly, 15 μ g of protein sample was loaded onto Phos-tag gels and run in Phos-tag SDS-PAGE electrophoresis buffer (50 mM Tris base, 50 mM MOPS, 0.1% [w/v] SDS, 5 mM sodium bisulfite, pH 7.2) 150 V for 90 min at room temperature. The resolving layer was equilibrated in Phos-tag transfer buffer (1 \times NuPAGE transfer buffer (Life Technologies #NP0006-1), 20% (v/v) methanol, 2.5 mM sodium pyrophosphate, 5 mM sodium bisulfite) for 15 min at room temperature with shaking. Proteins were then transferred to polyvinylidene difluoride (PVDF) membranes (Millipore #IPVH00010) in Phos-tag transfer buffer at 20 V for 20 hrs at 4°C.

Membranes were placed in Phos-tag blocking buffer composed of TBS-T with 2% (w/v) fish gelatin and 10 mM NaN₃ for 1 hr at room temperature. Membranes were then probed simultaneously with the Fus3 and Myc primary antibodies (detailed above) in TBS-T containing 0.5% fish gelatin and 10 mM NaN₃. Blots were washed 3 \times 5 min with TBS-T, then incubated with donkey anti-goat Alexa-647 (Thermo Life Sciences # A-21447, 1:1,000 ratio) and donkey anti-mouse Alexa-555 (Thermo Life Sciences #A-31570, 1:1,000 ratio) secondary antibodies in TBS-T containing 0.5% fish gelatin, and then washed 3 \times 5 minutes with TBS-T at room temperature. MAPK blots were imaged on a Bio-

Rad ChemiDoc MP imaging system using multichannel acquisition mode (Fus3, Alexa 647 channel; Kss1-Myc, Alexa546 channel) optimizing for intense bands after washing off excess secondary antibodies. Blots were stripped and re-probed with G6PDH primary antibodies, HRP-conjugated goat anti-rabbit secondary antibodies, and imaged with Clarity ECL Western Blotting Substrate (Bio-Rad #1705061), as described above.

2.5 | Image densitometry

Densitometry analysis was carried out in ImageJ (Schneider, Rasband, & Eliceiri, 2012) as described previously (Janes, 2015). Briefly, 16-bit raw TIF files were exported from the Bio-Rad Image Lab software and opened in ImageJ. Images were rotated to align bands horizontally, and the rectangle tool was used to select each lane for analysis. Rectangles were drawn to cover the entire width of the band in one lane without causing overlap in other lanes and were drawn long enough to sample the background pixel intensities surrounding the band(s) of interest. Pixel intensity profiles were plotted, and background was subtracted by connecting the adjacent background intensities surrounding the peak corresponding to the band of interest using the line tool. The left and right sides of the peaks of interest were connected to the horizontal line created for background subtraction, effectively isolating roughly 95% of the Gaussian distribution. The magic wand tool was then used to obtain the area under the curve as the raw densitometry value. For phospho-p44/42 data, the percent phosphorylated MAPK from total MAPK was calculated using densitometry values that were normalized to the loading control. For Phos-tag data, raw densitometry values were used to determine the percent of total MAPK that was phosphorylated. The values for each band in a given lane were totalled, and the corresponding percent of the total was calculated for each band. Protein induction over time (t-MAPK) was calculated by normalizing the total MAPK signal to the loading control as for the phospho-p-44/42 data.

2.6 | Population-based transcriptional reporters

Wild-type, Kss1-Myc, and *bar1Δ* Kss1-Myc strains were transformed with pRS423-P_{FUS1}-LacZ or pRS426-P_{FUS1}-YeGFP3. Four colonies from each transformation were grown at 30°C to saturation overnight in selection medium, and then diluted to OD₆₀₀ = 0.2 the following day and grown to OD₆₀₀ ~ 0.6–0.8. These cultures were again diluted to OD₆₀₀ = 0.005 and grown overnight to OD₆₀₀ ~ 0.8. Ninety microlitres were added per well in duplicate rows to black clear-bottomed 96-well plates (Corning Costar) containing 10 μl of 10× stocks of serially diluted α-factor mating pheromone prepared in sterile water, with one well per row containing 10 μl of sterile water only. P_{FUS1}-GFP measurements were carried out as described previously (Shellhammer et al., 2017). Briefly, samples were incubated for 1.5, 2, 2.5, and 3 hr at 30°C. GFP fluorescence was measured using a Molecular Devices Spectramax i3x plate reader at an excitation wavelength of 483 nm and emission wavelength of 518 nm. The OD₆₀₀ was

measured at each time point to determine cell density. P_{FUS1}-LacZ assays were carried out as described previously (Hoffman, Garrison, & Dohlman, 2002). Briefly, samples were incubated for 1.5 hr at 30°C. The OD₆₀₀ for each well was measured to determine cell density after which 20-μl fluorescein di-β-D-galactopyranoside (FDG) solution (135 mM PIPES, 0.25% [v/v] Triton X-100, 0.5 mM FDG, pH 7.2) was added to each well. After 1.5 hr at 37°C, the reaction was stopped by addition of 20 μl of 1 M sodium carbonate, and fluorescence was measured using a Molecular Devices Spectramax i3x plate reader at an excitation wavelength of 485 nm and emission wavelength of 580 nm.

For data analysis and presentation, raw fluorescence values from each well were normalized to the number of cells in that well (represented by the OD₆₀₀) using the shorthand Taylor Series 1/(1 + x) where x = OD₆₀₀. Normalized values of each technical duplicate were averaged. Finally, each well was normalized as a percent of the average maximum fluorescence value in the wild-type strain. Dose-response curves were fitted to the data using a non-linear Boltzmann function using a least squares regression in GraphPad Prism 4.

2.7 | Flow cytometry

Wild-type, *bar1Δ*, and *gpa1^{G302S}* strains with integrated P_{FUS1}-GFP and P_{ADH1}-mCherry transcriptional reporters (Dixit et al., 2014) were grown as described above for the population-based transcriptional reporter assays. Forty-five microlitres from each culture were added to each well in duplicate rows to black clear-bottomed 96-well plates (Corning Costar) containing 5 μl of 10× stocks of serially diluted α-factor mating pheromone. The cells were then incubated in a shaker at 30°C for 1.5 hr. For experiments where BSA-coated plates were used, each well was filled completely with 1% BSA solution in sterile-filtered water and incubated at 4°C overnight. The liquid was removed before filling the plate for experiments.

For live-cell flow cytometry, the plates were placed on ice after 1.5 hr and analysed within 15 min. For fixed-cell flow cytometry, a stock solution of cycloheximide (400 μg/ml) was added to each well to a final concentration of 4 μg/ml. Then plates were centrifuged (500 × g) for 2 min at room temperature. The supernatant was removed, and the cells were resuspended in 50 μl of paraformaldehyde solution (1 M phosphate buffer, 2% paraformaldehyde, 4 μg/ml cycloheximide, pH 7.5). The cells were incubated in paraformaldehyde solution for 15 min at 20°C. After incubation, the plate was centrifuged (500 × g) for 2 min at room temperature. The supernatant was removed, and the cells were resuspended in 50 μl of wash buffer (1 M phosphate buffer, 75 mM lysine mono-HCl, 4 μg/ml cycloheximide, pH 7.5). Cells were washed once more in this buffer and stored at 4°C in the dark for up to 5 days.

The height and area of the peaks for side scatter (SSC), forward scatter (FSC), green fluorescence (GFP), and red fluorescence (mCherry) were measured using an Intellicyt iQue Screener PLUS equipped with three lasers (405, 488, and 561 nm). All flow cytometry

data analysis was performed using the FlowCytometryTools Python package (Friedman & Yurtsev, 2017). First, cells were gated based on the heights of their forward and side scatter peaks (Figure S3a) to isolate cells from debris. This population was then gated based on positive mCherry fluorescence intensity (Figure S3b) to remove any additional debris or dead cells that did not have mCherry expression. Finally, any cells with negative values for GFP fluorescence were removed (Figure S3c).

The transcriptional response was quantified as GFP fluorescence divided by mCherry fluorescence. By normalizing with a constitutively active transcriptional reporter such as P_{ADH1} -mCherry, we can account for differences in protein expression and distinguish doublets and singlets. It is also possible to normalize by forward-scatter as a surrogate measurement of cell size (Figure S3d). We use mCherry fluorescence because it also accounts for cell-to-cell differences in protein expression. For each strain and dose of pheromone, we calculated the mean and standard deviation of the mCherry-normalized GFP fluorescence. Any cells that were two or more standard deviations above or below the mean were considered outliers and removed from subsequent analysis. Data were reported as the median of the normalized GFP fluorescence of the remaining cells. Dose-response curves were fitted to a nonlinear Boltzmann function in GraphPad Prism 4 using a least squares regression.

2.8 | Imaging cytometry

Cells were prepared for imaging cytometry as described above for flow cytometry but using half-area, black, clear-bottomed 96-well plates (Greiner CELLSTAR). Each plate of cells was then centrifuged at $500 \times g$ for 5 min at 4°C. Cells were imaged in a Nexcelom Celigo S every 20 min for 3 hr at room temperature using the "Target 1 + Mask" expression analysis settings. Target 1 was GFP (green channel), and the brightfield image was used as a mask to segment cells. Exposure time for GFP was 200,000 μ s.

The cells were segmented using Celigo's native brightfield algorithm for image analysis. The intensity threshold was set to 10, the precision was set to high, the cell diameter and dilation radius were set to 4 μ m and 0 μ m, respectively, and the separate touching objects setting was turned on. The identified cells were then gated based on the mean intensity and aspect ratio of mCherry fluorescence to exclude debris and clumps of cells (Figure 5a). Background correction was used in the analysis of the GFP intensity. For data analysis and presentation, the mean GFP intensity was averaged across three to four biological replicates. Dose-response curves were fitted to a non-linear Boltzmann function in GraphPad Prism 4 using a least squares regression.

2.9 | Microfluidics chamber assembly

Polydimethylsiloxane (PDMS) was prepared by combining 36 g of base with 4 g of curing agent (from the Dow Sylgard 184 silicone elastomer kit) in a polystyrene weigh boat and mixing for 2 min.

The PDMS mixture was then poured over the mould in a second polystyrene weigh boat and placed in a vacuum chamber for 1 hr to remove any bubbles. The PDMS was then cured overnight at 68–70°C. The sides of the weigh boat were cut away and gently separated from the PDMS and mould. Then the PDMS was separated from the mould by gently cutting around the edge of the mould with scissors. The feature side of the PDMS was protected with clear tape before individual chambers were cut out using a razor blade. The locations of the ports were marked on the tape with a permanent marker pen. The ports (schematic in Figure S4b) were created by pushing a 0.5-mm puncher (World Precision Instruments) through the non-feature side of the PDMS. The puncher was carefully removed by holding the chamber down with forceps and pulling the puncher straight up. The chamber was cleaned three to four times using clear tape and then washed sequentially with ACS grade methanol, 70% ethanol diluted in filtered deionized water, and filtered deionized water. The chamber was then blown dry with air and placed in a clean petri dish with the features facing up. A glass slide was cleaned following the same protocol. Both the chamber and the glass slide must be very clean to ensure complete fusion of the chamber to the coverslip. Next, the chamber and cover slip were placed in a plasma cleaner (Harrick Plasma PDC-32G) with the feature side of the chamber facing up and run for 30–45 s to replace the Si-CH₃ bonds with Si-OH bonds (Figure S4a). Then the chamber was placed on top of the cover slip with the feature side facing down. When the PDMS and the glass come in contact with each other, they fuse by forming covalent Si-O-Si bonds (Figure S4a). The chamber typically fused instantly; however, sometimes, it was necessary to push down on the corner of the chamber, avoiding the features, to start fusion. The chamber was then placed at 58–60°C for 2 hr to complete fusion.

Each experiment required eight syringes and lines. Each line was prepared by inserting a 23-gauge needle into one end of 1–2 meters of (Cole-Palmer Tygon) tubing with inner diameter of 0.020 in., outer diameter of 0.060 in., and a 23-gauge Luer stub into the other end. The lines were connected to syringes by screwing the syringe into the Luer stub. Seven lines were prepared with plain medium (SCD), and one line was prepared with SCD containing mating pheromone and a 1:1,000 dilution of stock Alexa Fluor 647 (Invitrogen) dye to visualize the presence of pheromone in the mating chamber.

To set up for imaging, the chamber was first secured to the stage with a slide holder. Then each line was inserted into the chamber; the line containing pheromone and dye was added last. As each line was added, some media was pushed through the chamber using a syringe to check for leaks. Once the chamber was set up, the cells were loaded gravitationally by holding the load syringe containing cells at ~0.100 OD above the shunt and tapping the side of the syringe. It is important to not push the cells in using the syringe as this will force the cells into the channels on either side of the chamber. The chamber was designed based on the dial-a-wave design, allowing the source of media to be switched to an input containing pheromone after two time points (Bennett et al., 2008).

2.10 | Microfluidics and time-lapse microscopy for the Bem1-GFP polarity reporter

For gradient experiments, Bem1-GFP was used to visualize the polar cap. The chamber was set up so that only one of the four input channels contained pheromone and dye, producing a gradient of pheromone. For these experiments, we used pheromone concentrations matched to the sensitivity of the individual strains: 0–150 nM for wild-type, 0–50 nM for *gpa1*^{G302S}, and *bar1Δ*. Time-lapse microscopy was performed using a Nikon Ti-E inverted fluorescence microscope with Perfect Focus, coupled with Hamamatsu Orca-flash 4.0 digital camera and a Lumen Dynamics C-Cite LED light source system. Images were taken using a Nikon Plan Apo VC X60 oil immersion objective (NA 1.40 WD 0.17 MM). Images were taken every 10 min in the brightfield, far-red, and green channels. The lowest LED intensity setting was used to prevent photobleaching and phototoxicity. Cells were imaged for 10 hr, and the first two time points were always taken in the absence of pheromone.

Images from microfluidics experiments were registered using the descriptor-based series registration (2d/3d + t) plugin based on the DIC images in ImageJ. The movement of the polar cap, as marked by Bem1-GFP, was tracked using the manual tracking plugin in ImageJ. Plots of the single polar cap traces and polar histograms of the angle of the traces were generated in Python using matplotlib. Cells were segmented based on the GFP images in ImageJ, and kymographs of the GFP intensity around the edge of a cell were generated in Matlab using code available on the GitHub repository. Segmentation was checked manually.

2.11 | Microfluidics and time-lapse microscopy for the Fus3 activity reporter

The experimental set-up for microfluidics devices was performed as described previously (Jiang, AkhavanAghdam, Tsimring, & Hao, 2017; Li, Roberts, et al., 2017). Time-lapse microscopy experiments were performed using a Nikon Ti-E inverted fluorescence microscope with Perfect Focus, coupled with an EMCCD camera (Andor iXon X3 DU897) and Spectra X LED light source system. Images were taken every 2 min in each fluorescence channel using a CFI Plan Achromat Lambda DM X60 oil immersion objective (NA 1.40 WD 0.13 MM).

Fluorescence images were processed as described previously (Li, Roberts, et al., 2017). The cytoplasm and the nucleus of single cells were identified by thresholding the phase image and the iRFP nuclear marker. For each individual cell, the mean fluorescence intensities for the cytoplasm and the nucleus were then quantified and smoothed separately, using a custom MATLAB code, as described in previous studies (AkhavanAghdam et al., 2016; Hansen, Hao, & O'Shea, 2015; Hao, Budnik, Gunawardena, & O'Shea, 2013; Hao & O'Shea, 2011). The ratio of the cytoplasmic to nuclear intensity (KTR C/N ratio) was calculated.

2.12 | Statistical analysis

All data are reported as mean \pm the standard deviation.

2.13 | Availability of data and material

All code used for analysis along with a selection of data from this work is available on GitHub at github.com/aeallen/pher-response-quantification. All data are available from the corresponding author on reasonable request.

3 | RESULTS

3.1 | PART I: Population-based assays of pheromone signalling

3.1.1 | Quantification of MAPK activity by immunoblotting with phospho-MAPK antibodies

Upon pheromone binding to the receptor, Gpa1 releases GDP, binds GTP, and dissociates from the G protein $\beta\gamma$ subunit complex (Figure 1). $G\beta\gamma$ can then activate multiple downstream effectors and trigger coordinated changes in protein phosphorylation, new gene transcription, cell cycle arrest, polarized cell expansion, and—ultimately—cell–cell fusion. More specifically, $G\beta\gamma$ promotes the activation of a protein kinase cascade that culminates with the phosphorylation and activation of two terminal MAPKs, Fus3, and Kss1 (Wang & Dohlman, 2004). It has long been recognized that MAPKs must be phosphorylated on two “activation loop” residues in order to achieve full catalytic activity and that these residues are conserved in yeast and humans (Ferrell & Bhatt, 1997; Haystead, Dent, Wu, Haystead, & Sturgill, 1992; Hur et al., 2008). This dual phosphorylation alters the conformation of the protein, thereby enabling ATP to bind to the catalytic site (Canagarajah, Khokhlatchev, Cobb, & Goldsmith, 1997).

Activation of the MAPKs is commonly determined by immunoblotting with antibodies raised against a phosphorylated activation loop peptide (phospho-p44/42). Although designed to recognize mammalian phospho-ERK1 and phospho-ERK2, they also recognize phospho-Fus3 and phospho-Kss1. In addition to Fus3 phosphorylation, *FUS3* transcription is induced by pheromone, resulting in an increase in Fus3 protein levels over time (Choi, Kim, Kim, Lee, & Choi, 2000; Elion, Grisafi, & Fink, 1990). To account for changes in Fus3 abundance, blots may be stripped of the phospho-specific antibodies and re-probed with antibodies against the total protein. Where commercial antibodies are unavailable, it is convenient to use an epitope-tagged version of the kinase of interest. Here, we used commercial polyclonal antibodies to quantify Fus3 and monoclonal antibodies to quantify epitope-tagged Kss1 (Kss1-Myc). Given the difficulty of resolving bands for large and/or heavily phosphorylated proteins, small epitope tags should be used whenever possible.

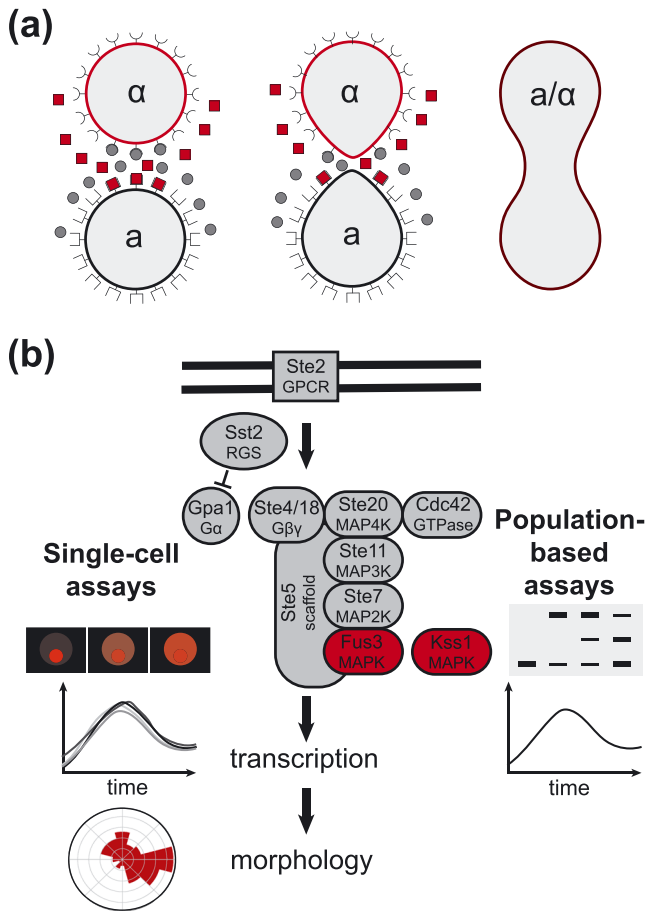


FIGURE 1 Schematic of pheromone response pathway. (a) Diagram of an *a* and an α cell mating to form an *a/α* diploid. (b) Representation of population-based and single cell assays that quantify each level of the pheromone response

To illustrate the phospho-specific antibody method, we measured Fus3 phosphorylation in wild-type and *bar1Δ* cells exposed to either low (0.3 μ M) or high (3 μ M) dose of pheromone. In wild-type cells treated with the low dose, Fus3 reached ~80% of maximal phosphorylation by 5 min and then decreased to ~30% of maximum by 90 min (Figure 2a, p-Fus3). At the high dose, the signal increased sharply at 5 min and then continued to increase for the duration of the experiment. Thus, two different doses may produce identical kinase activation at a single (early) time point but nevertheless exhibit dramatic differences in the duration and final level of kinase activation, as reported previously (Hao et al., 2008). In comparison, the response in *bar1Δ* cells was sustained at both pheromone concentrations (Figure 2b, p-Fus3). Other supersensitive mutants (*sst2Δ*, *sst2*^{Q304N} and *gpa1*^{G302S}) also exhibit prolonged MAPK phosphorylation, even after pheromone removal (Dixit et al., 2014).

Part of the increase in Fus3 phosphorylation is due to an increase in Fus3 expression. To account for this, we stripped the blots and re-probed with Fus3 antibodies. In both wild-type and *bar1Δ* mutant cells, subjected to either dose of pheromone, the abundance of Fus3 increased substantially within 30 min and then increased more gradually for the remainder of the experiment (Figure 2a,b, t-Fus3).

Although Fus3 induction was similar in wild-type and mutant cells (Figure 2b, t-Fus3), the proportion of Fus3 that was phosphorylated diminished more quickly in the wild-type strain, particularly at the low dose of pheromone (Figure 2a,b, p-Fus3:t-Fus3). Therefore, Bar1 limits Fus3 phosphorylation, but not Fus3 induction, and the difference between the mutant and wild-type strains is most evident at lower doses of pheromone. Collectively, these data are consistent with the fact that Bar1 degrades α -factor and dampens the downstream signal over time (Banderas, Koltai, Anders, & Sourjik, 2016; Barkai et al., 1998; Chan & Otte, 1982b; Chen, Nie, Yi, & Chou, 2016; Diener et al., 2014; Jackson & Hartwell, 1990a; Jin et al., 2011; Segota & Franck, 2017).

3.1.2 | Quantification of MAPK activity by Phos-tag SDS-PAGE and immunoblotting

Although relative changes in phosphorylation can be determined using phospho-specific antibodies, it is now appreciated that Fus3 exists in both mono-phosphorylated and dually phosphorylated pools (Bhattacharyya et al., 2006; Nagiec et al., 2015) and that the phospho-p44/42 antibodies are able to detect, to an extent, mono-phosphorylated Fus3 (Hur et al., 2008). This is a concern because mono-phosphorylated Fus3 does not stimulate, but rather inhibits, downstream signalling (Nagiec et al., 2015). Results using phospho-p44/42 antibodies are, therefore, only an approximation of kinase activation. In the following section, we describe the use of Phos-tag gel electrophoresis to determine the stoichiometry of MAPK phosphorylation.

Phosphate-binding tag, or Phos-tag, is a divalent-metal-coordinating small molecule that has a high affinity for phosphorylated serine, threonine, and tyrosine (Kinoshita, Kinoshita-Kikuta, Takiyama, & Koike, 2006; Kinoshita-Kikuta, Aoki, Kinoshita, & Koike, 2007). By adding Phos-tag and a divalent metal (i.e., Mn^{2+} or Zn^{2+}) to acrylamide gels, the electrophoretic mobility of phosphorylated proteins is slowed, thereby enhancing the separation of phosphorylated and non-phosphorylated species. Probing with antibodies specific to the protein of interest (e.g., Fus3) allows a ratiometric quantification of each phospho-species in the same blot. Thus, the number of bands is proportional to the number of phosphorylation events on the protein. We have used Phos-tag SDS-PAGE and immunoblotting to identify a substantial pool of mono-phosphorylated Fus3 in the cell (Nagiec et al., 2015). Moreover, we have used a series of functional assays (such as those described below) to assign a negative regulatory role to that form of the protein.

To illustrate the data that can be collected by the Phos-tag method, we reanalysed the samples used above (Figure 2). As shown in Figure 3, we obtained clear separation of dually phosphorylated, mono-phosphorylated, and non-phosphorylated Fus3 (Figure 3, blots). In either strain, and at both high and low doses, 20–30% of Fus3 became dually phosphorylated and a similar proportion became mono-phosphorylated. With the exception of the wild-type strain treated with low pheromone, the two phosphorylated species persisted for the remainder of the time course (Figure 3a,b, Fus3).

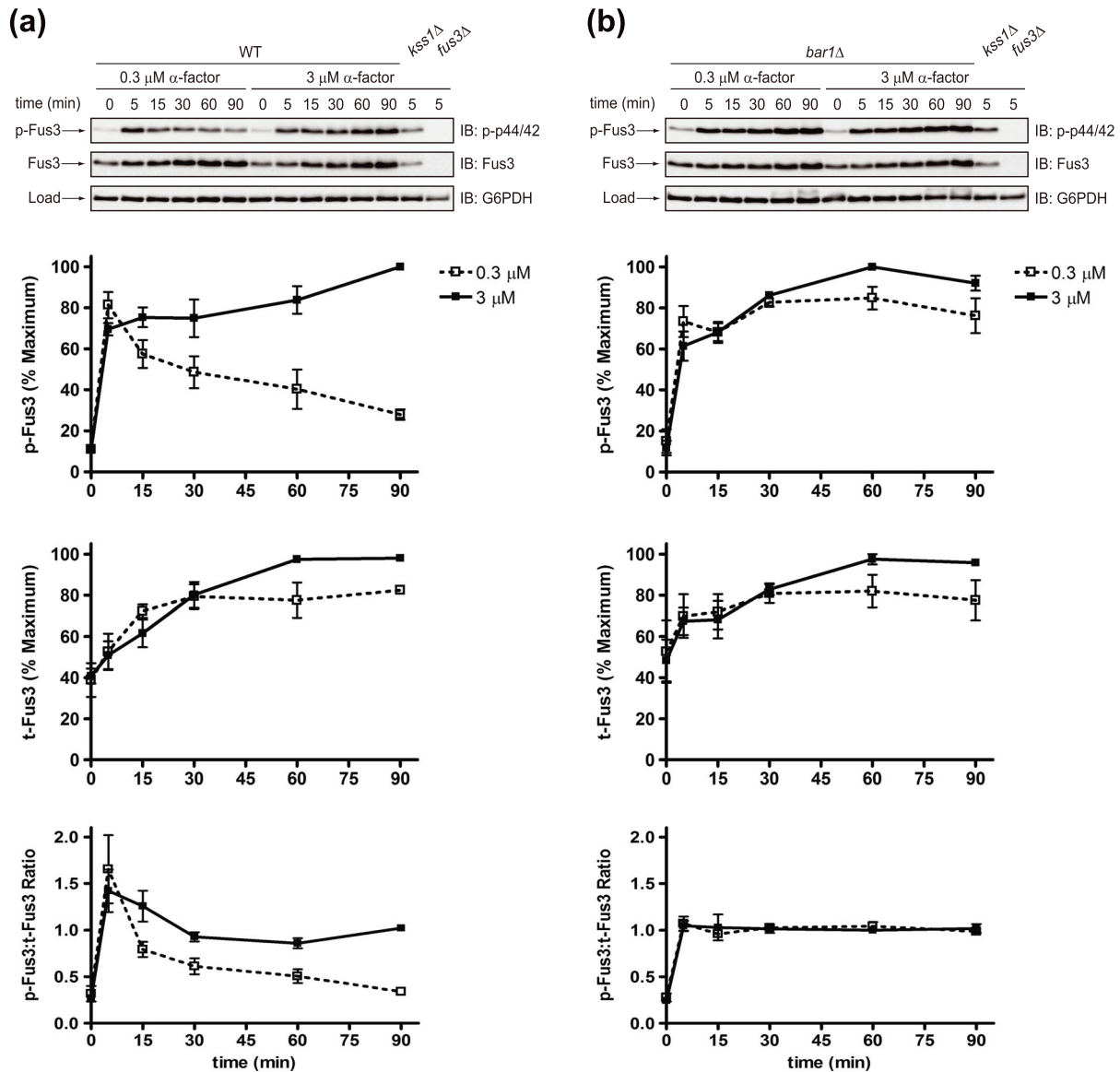


FIGURE 2 Phosphorylation of Fus3 by conventional SDS-PAGE and immunoblotting with phospho-p44/42 antibodies. Western blot analysis of (a) wild-type cells or (b) *bar1Δ* cells treated with 0.3 μM or 3 μM α-factor mating pheromone and probed with phospho-p44/42 and total Fus3 antibodies. Phosphorylated Fus3 (p-Fus3) and total Fus3 (t-Fus3) were plotted as % of maximum signal on the blot. The ratio of phosphorylated Fus3 to total Fus3 (p-Fus3:t-Fus3) was calculated by dividing % phosphorylated Fus3 by % maximum total Fus3. Data are presented as mean ± standard deviation, $N = 3$ [Colour figure can be viewed at wileyonlinelibrary.com]

To account for changes in Fus3 abundance, we summed the intensities of all three bands for each lane and calculated the proportion of total protein that underwent dual phosphorylation. By this method, the dose-dependent differences for wild-type mirrored those seen using phospho-specific antibodies (Figure 2, p-Fus3). However, in contrast to the results shown in Figure 2, dual-phosphorylation in the mutant strain was transient. As shown in Figure 3b (ppFus3:t-Fus3), activity peaked at 5 min and then diminished over time, in a manner similar to that seen in wild-type. These data are consistent with earlier data showing that part of the phospho-specific antibody signal is due to detection of mono-phosphorylated Fus3 (Figure 2a, p-Fus3). As with any analysis of protein phosphorylation, proper controls are essential. To illustrate, we have shown previously that mutations in the

activation loop phosphorylation sites (T180A and Y182F) eliminate individual bands detected by the Fus3 antibody (Nagiec et al., 2015).

It is well established that pheromone promotes the phosphorylation of Kss1, as well as Fus3, as originally shown using phospho-specific antibodies (Sabbagh, Flatauer, Bardwell, & Bardwell, 2001; Figure S1). However, previous Phos-tag analysis, done in another yeast strain (W303), did not detect a mono-phosphorylated form of Kss1 (Winters & Pryciak, 2018), most likely due to insufficient resolution from unphosphorylated Kss1 in those gels. To compare the behaviours of the two kinases directly, we probed the original blots simultaneously with anti-Fus3 rabbit and anti-Myc mouse antibodies; we then probed with secondary antibodies conjugated to different fluorophores. Such multi-channel imaging allows detection of multiple

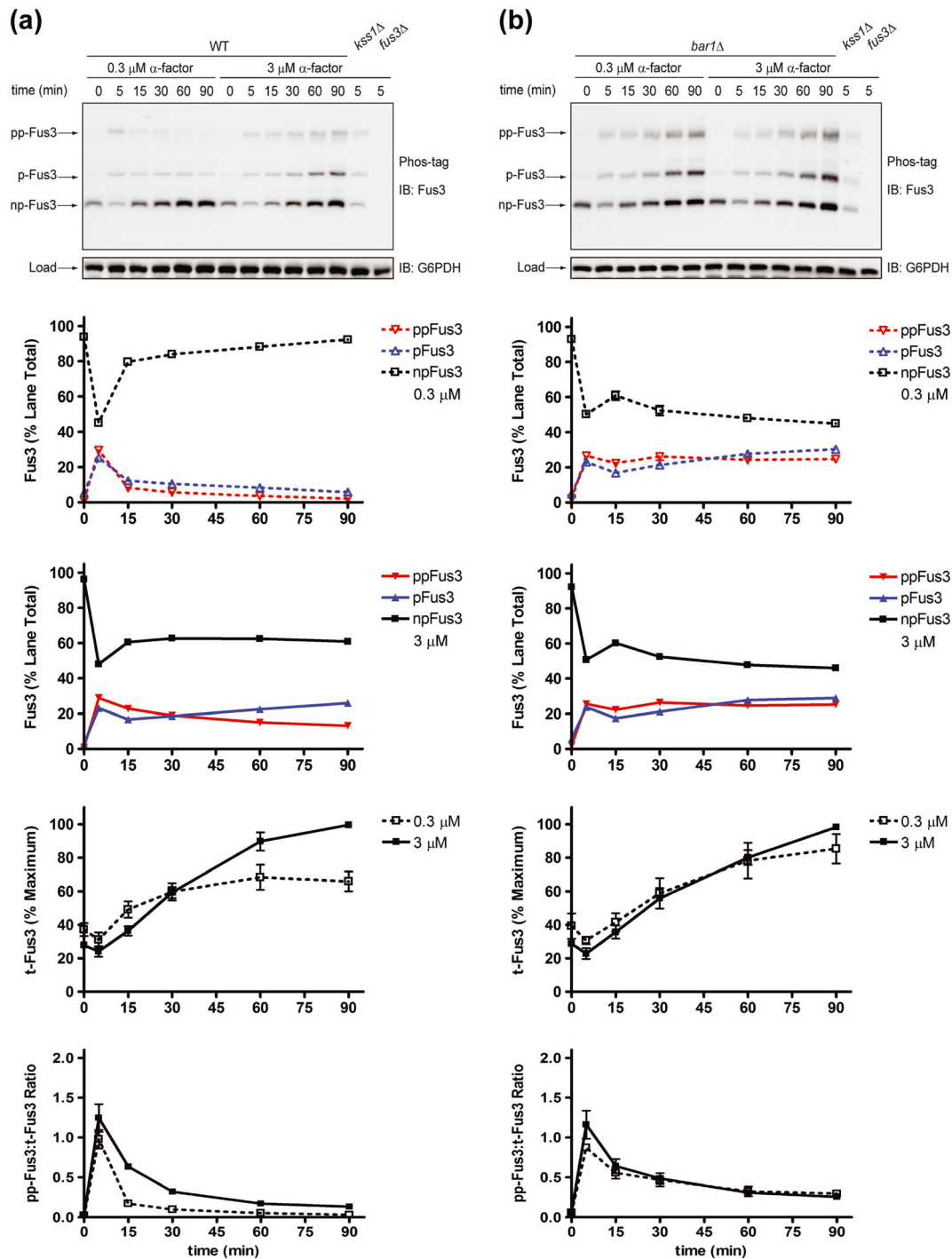


FIGURE 3 Phosphorylation of Fus3 by Phos-tag SDS-PAGE and immunoblotting with Fus3 antibodies. Phos-tag western blot analysis of (a) wild-type cells or (b) *bar1* Δ cells treated with 0.3 μ M or 3 μ M α -factor mating pheromone and probed with total Fus3 antibodies to identify dually-phosphorylated (pp-Fus3), mono-phosphorylated (p-Fus3), and non-phosphorylated (np-Fus3) Fus3. pp-Fus3, p-Fus3, and np-Fus3 (Fus3) are plotted as % of lane total. Total Fus3 (t-Fus3) is plotted as % maximum lane signal on the blot. The ratio of dually phosphorylated Fus3 to total Fus3 (pp-Fus3:t-Fus3) was calculated by dividing the % dually phosphorylated Fus3 in each lane by % total Fus3 in each lane. Data are presented as mean \pm standard deviation, $N = 3$

proteins under identical experimental conditions. As shown in Figure S2, and as shown previously for Fus3, Phos-tag analysis revealed a pool of dually phosphorylated, mono-phosphorylated, and non-phosphorylated Kss1 (Figure S2). Moreover, dual phosphorylation of Kss1 reached 50–60% of the total protein, substantially more than

that observed for Fus3. Thus, results for Kss1 obtained by the Phos-tag method mirrored those obtained by conventional immunoblotting. It is unclear why the proportion of phosphorylated Kss1 is greater than that of Fus3. At this point, we can only speculate on the cause or consequences of this difference.

3.1.3 | Quantitative transcription-reporter assays

Activation of Fus3 and Kss1 leads to direct phosphorylation of the transcription factor Ste12 (Breitkreutz, Boucher, & Tyers, 2001; Elion, Satterberg, & Kranz, 1993; Hung, Olson, Breitkreutz, & Sadowski, 1997; Song, Dolan, Yuan, & Fields, 1991), a repressor complex consisting of Dig1 and Dig2 (Bardwell, Cook, Zhu-Shimoni, Voora, & Thorner, 1998; Cook, Bardwell, Kron, & Thorner, 1996; Madhani, Galitski, Lander, & Fink, 1999; Roberts et al., 2000; Tedford, Kim, Sa, Stevens, & Tyers, 1997), and a competing transcription factor Tec1 (Bao, Schwartz, Cantin, Yates, & Madhani, 2004; Brückner et al., 2004; Chou, Huang, & Liu, 2004; Wang & Dohlman, 2004). These events induce a number of genes required for mating (Breitkreutz et al., 2001; Madhani et al., 1999; Roberts et al., 2000). Thus, any differences in MAPK activation can be interpreted in light of downstream outputs such as transcription induction.

Among the most strongly induced genes is *FUS1*, which is also highly specific to the pheromone pathway (Hagen et al., 1991). Accordingly, the *FUS1* promoter is widely used as an indicator of pheromone-dependent gene expression (Erdman et al., 1998; Hoffman et al., 2002; McCaffrey, Clay, Kelsay, & Sprague, 1987; Trueheart, Boeke, & Fink, 1987) and has been fused to reporter genes that encode β -galactosidase and fluorescent proteins (e.g., GFP), as well as drug resistance and nutritional markers (Mentesana, Dosil, & Konopka, 2002). The β -galactosidase reporter assay has been the standard for decades, and enzyme expression can be readily detected through cleavage of a suitable substrate. Measurement of ortho-nitrophenyl- β -galactoside cleavage requires cell disruption and is no longer widely used (Sprague, 1991), having been replaced by the cell permeable substrate fluorescein di-D-galactopyranoside (Hoffman et al., 2002). Whereas the former relies on a colorimetric readout, the latter produces a product that is fluorescent and thus substantially more amenable to quantitation.

To illustrate the method, we compared wild-type and *bar1* Δ cells treated with a range of pheromone concentrations in 96-well microplates. Cells were grown to early log phase, stimulated with pheromone for 90 min, and then combined with the substrate FDG. After an additional 90 min, the reaction was stopped by addition of sodium carbonate. Substrate cleavage was determined in a microplate spectrophotometer and reported as the percent maximum fluorescence emission (485 nm excitation, 580 nm emission) normalized to optical density (600 nm, a surrogate measure of cell density). As shown in Figure 4a, wild-type cells reach a maximum response at approximately 10 μ M α -factor, with an EC₅₀ of \sim 1 μ M. Cells lacking Bar1 were approximately tenfold more sensitive than wild-type cells.

We obtained similar results using an alternative construct where the *FUS1* promoter drives expression of GFP (Figure 4b). In this experiment, cells in early log phase were stimulated with pheromone and monitored after 90 min and every 30 min thereafter. GFP induction was determined in a microplate spectrophotometer (483 nm excitation, 518 nm emission). OD₆₀₀ was measured at each time point to determine cell density. Importantly, the GFP method can be used to take multiple measurements of the same sample and, as discussed

below, of the same cell over time. As shown in Figures 4c (wild-type) and 3d (*bar1* Δ), the maximum GFP signal increased over time, from roughly fivefold over basal after 1.5 hr to \sim 15-fold by 3 hr. By comparison, the β -galactosidase signal was approximately 50-fold over basal after 1.5 hr. Thus, the enzyme-based assay has a higher dynamic range than that of the GFP method. While this is not a concern with the strongly induced *FUS1* promoter, it may limit the ability to work with some promoters.

3.2 | Part II: Single-cell assays of pheromone signalling

3.2.1 | Overview

Most cellular assays provide an averaged measure of the population at a single point in time. However, there is a growing appreciation of the prevalence and importance of cell-to-cell variability (or "noise") in biological processes. Such differences can arise from stochasticity in biochemical reactions, differences in the expression or activity of internal signalling components, age-dependent accumulation of aggregated or damaged proteins, perturbations in membrane trafficking, and asynchronous progression through the cell cycle (Ansel et al., 2008; Beckskei, Kaufmann, & van Oudenaarden, 2005; Colman-Lerner et al., 2005; Elowitz, Levine, Siggia, & Swain, 2002; Fraser, Hirsh, Giaever, Kumm, & Eisen, 2004; Li et al., 2017; McAdams & Arkin, 1999; Paliwal et al., 2007; Pesce et al., 2018; Raser & O'Shea, 2004; Volfson et al., 2006; Yu et al., 2008). In that regard, fluorescent protein-based reporters have been particularly useful because they permit quantitative measurements of induction in single, living cells over time. Accordingly, our single-cell measurements use a genetically integrated reporter of transcription or a genetically integrated kinase translocation reporter (KTR) for Fus3 activation (Li, Roberts, et al., 2017). In addition to the wild-type and *bar1* Δ strains, we expanded our analysis to include strains expressing the Gpa1^{G302S} mutant. This mutation prevents binding to Sst2, thereby slowing G α GTPase activity and amplifying the pheromone response (DiBello et al., 1998). The *gpa1*^{G302S} allele has been shown previously to increase cell-to-cell variability in transcription and morphogenesis (Dixit et al., 2014).

3.2.2 | Quantitative transcription-reporter assays using flow cytometry

Flow cytometry is a method whereby cells in solution are passed, one cell at a time, through a laser beam and analysed for volume (forward-scattered light), morphological complexity (side-scattered light), and fluorescence intensity. Forward scatter and side scatter are surrogate measures of cell size and shape, respectively. The scatter data are plotted in two dimensions, and the single, intact cells are binned into "gates" for further quantification in a third dimension (e.g., fluorescence signal; Figure S3a). This method has long been used to monitor the expression of cell surface antigens using fluorescently tagged antibodies. Another common application is to measure DNA content for cell cycle analysis (Hutter & Eipel, 1978), including measures of cell

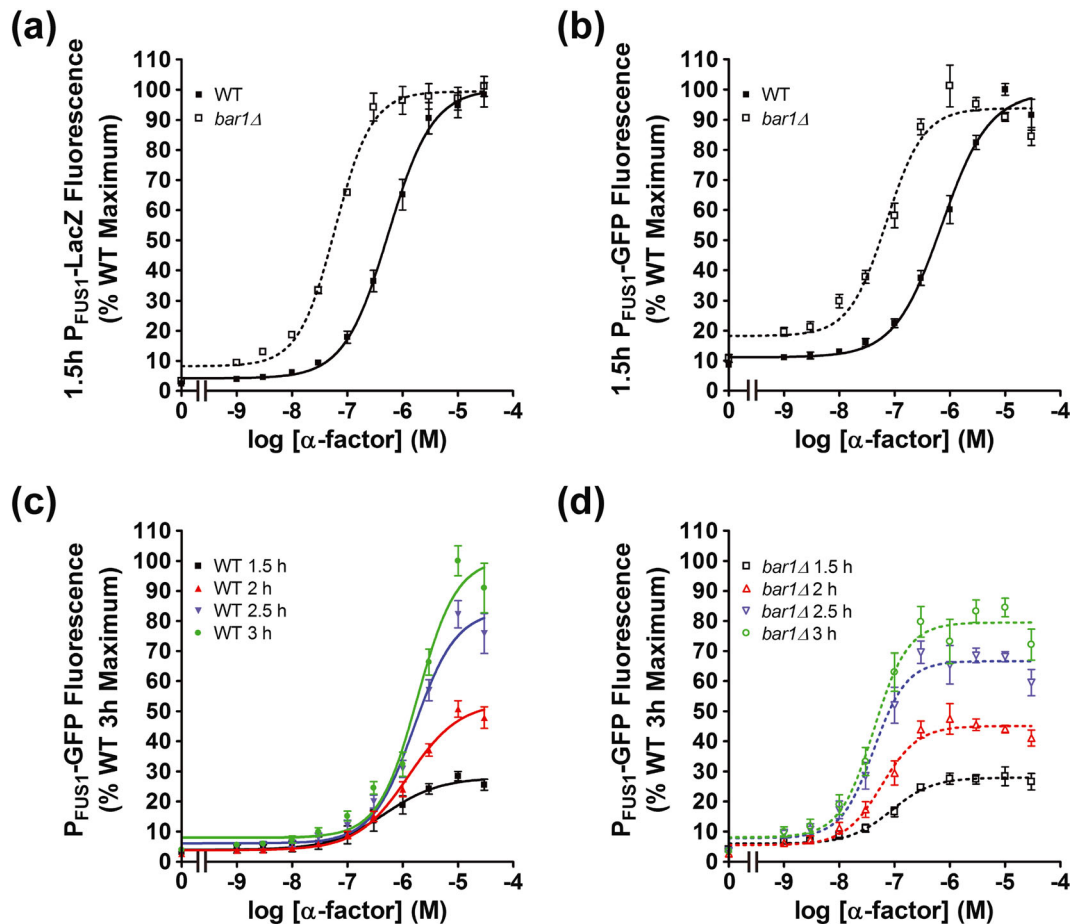


FIGURE 4 Pheromone-induced gene transcription assays. Dose–response curves for transcriptional output of wild-type and *bar1*Δ cells after 1.5 hr of treatment with α -factor mating pheromone, obtained by (a) the P_{FUS1} -LacZ and (b) the P_{FUS1} -GFP reporters. Time course of P_{FUS1} -GFP response in (c) wild-type cells and (d) *bar1*Δ cells. Data are presented as mean \pm standard deviation, $N = 4$

cycle arrest in response to mating pheromone (Pope & Pryciak, 2013). In that case, the readout is DNA content, and is therefore an indicator of the enrichment of haploid cells in either G1 (1N) or G2 (2N).

To monitor cell-to-cell differences, we typically use dual reporters, one composed of mCherry driven by the *ADH1* promoter and the other composed of GFP driven by the *FUS1* promoter. Whereas P_{ADH1} -mCherry is constitutively produced (Figure S3b), P_{FUS1} -GFP reports only pheromone-driven transcription (Figure S3c). Both reporters are integrated into the genome to avoid the cell-to-cell differences resulting from varied plasmid copy number. Normalizing a pathway-specific response (GFP) with a reference reporter (mCherry) accounts for differences in cell size, differences in protein expression capacity, and any day-to-day differences in instrument function. The underlying assumption is that the average amount of mCherry remains constant during progression through the cell cycle and is unaffected by any alterations in cell size or morphology. We then calculate the coefficient of variation (CV) for the population at discrete time points. This type of experimental platform allows us to measure pathway-specific noise and also to differentiate biochemical noise within a single cell (intrinsic noise) from variability within the population (extrinsic noise; Colman-Lerner et al., 2005; Dixit et al., 2014; Kelley et al.,

2015; McCullagh, Seshan, El-Samad, & Madhani, 2010; Pesce et al., 2018; Raser & O'Shea, 2004; Volfson et al., 2006).

To illustrate this method, we compared the normalized transcriptional response in wild-type cells under a variety of experimental conditions. Anecdotal evidence indicates that the apparent sensitivity to pheromone depends on whether the cells are maintained in glass or plastic, possibly because of binding of the α -factor peptide to the surface of microplates. Accordingly, we compared the P_{FUS1} -GFP response in plates that were either pretreated with bovine serum albumin (BSA), as a blocking agent, or left untreated. As shown in Figure 5 a, we observed a leftward shift in the EC_{50} in wild-type cells, from ~ 100 to ~ 10 nM as a result of BSA pretreatment. Similarly, the super-sensitive *bar1*Δ and *gpa1*^{G302S} mutants exhibited a leftward shift compared with wild-type cells (Figure 5b).

When a large number of conditions are being tested, or when instrument time is limited, it can be convenient to preserve the samples for later analysis. Accordingly, we compared living cells with cells that had been fixed with paraformaldehyde. As shown in Figure 5, we could observe both GFP and mCherry signals after fixation, albeit with an obvious difference in the slope of the dose–response curve. These findings highlight the distinction between receptor affinity and ligand

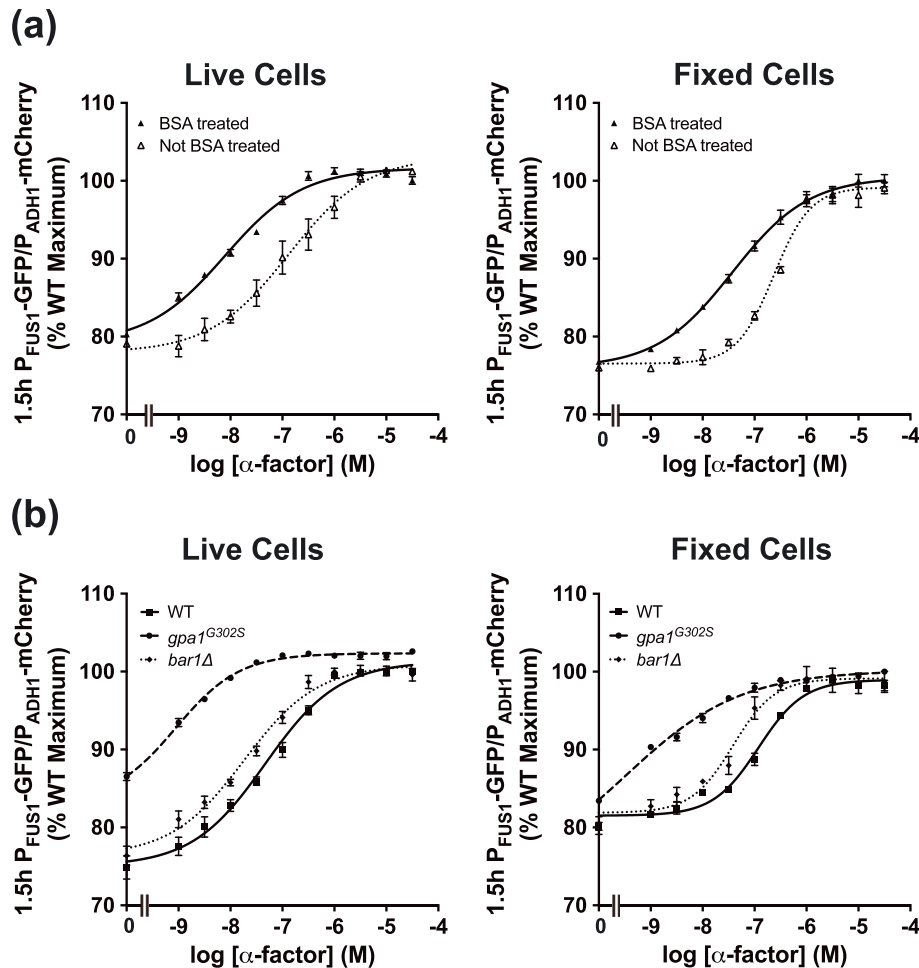


FIGURE 5 Flow cytometry transcription assays. Cells gated based on forward scatter, side scatter, and fluorescence (see Figure A3, a-c) were used for (a) dose–response experiments done with wild-type cells in wells that were either untreated or coated with BSA and analysed either immediately (live cells) or after chemical fixation. (b) Dose–response experiments done with wild-type, *gpa1*^{G302S}, and *bar1Δ* cells in BSA-coated wells were analysed immediately or after chemical fixation. Data were fitted using the sigmoidal dose–response in Prism (GraphPad). Data are presented as mean ± standard deviation, $N = 4$ [Colour figure can be viewed at wileyonlinelibrary.com]

potency. Whereas the former describes the binding affinity of one substance for another (K_d or K_a), potency describes the amount of substance required to produce a biological effect (EC_{50} or IC_{50}). Thus, we avoid drawing conclusions about “physiological concentrations” of pheromone based on data obtained in a non-physiological (laboratory) setting, particularly when comparing multiple distinct readouts of pathway activity. The distinction between receptor occupancy and downstream responses is also relevant to understanding the significance of “dose–response alignment” (Yu, Qi, Sheff, & Elion, 2008).

3.2.3 | Quantitative transcription-reporter assays using imaging cytometry

A limitation of flow cytometry is its inability to track individual cells over time. Thus, we have recently turned to imaging cytometry as an alternative approach. Imaging cytometers allow the user to monitor cell function in micro-well plates using brightfield and fluorescence channels. In these experiments, cells are prepared as described above for flow cytometry, except that the cells are not fixed and the plates

are not shaken, and we use half-area 96-well plates to reduce acquisition time. To quantify cellular response, we first identify the cells using Nexcelom’s proprietary brightfield segmentation algorithm. To identify individual cells, we gate all identified cells based on GFP fluorescence and aspect ratio (Figure 6a). We then determine the mean GFP fluorescence intensity for each cell. It is also possible to normalize by mCherry intensity, which results in a more normally distributed data set (Figure 6b). However, imaging cells for an extended time using the GFP and mCherry fluorescence channels is phototoxic. Therefore, we normalize based on cell size and do not capture images in the mCherry channel. As shown in Figure 6, the EC_{50} values obtained from imaging cytometry mirror those obtained by flow cytometry, although imaging cytometry has a somewhat higher dynamic range (compare Figures 4a with 5c, and 4b with 5c and 5d). As with flow cytometry, we observed a leftward shift in the dose–response profile when using BSA-treated plates (Figure 6c) or cells bearing the *bar1Δ* or *gpa1*^{G302S} mutations (Figure 6d).

An important advantage of imaging cytometry is the ability to repeatedly image the same cells over time (Figure 5e–g). This is useful

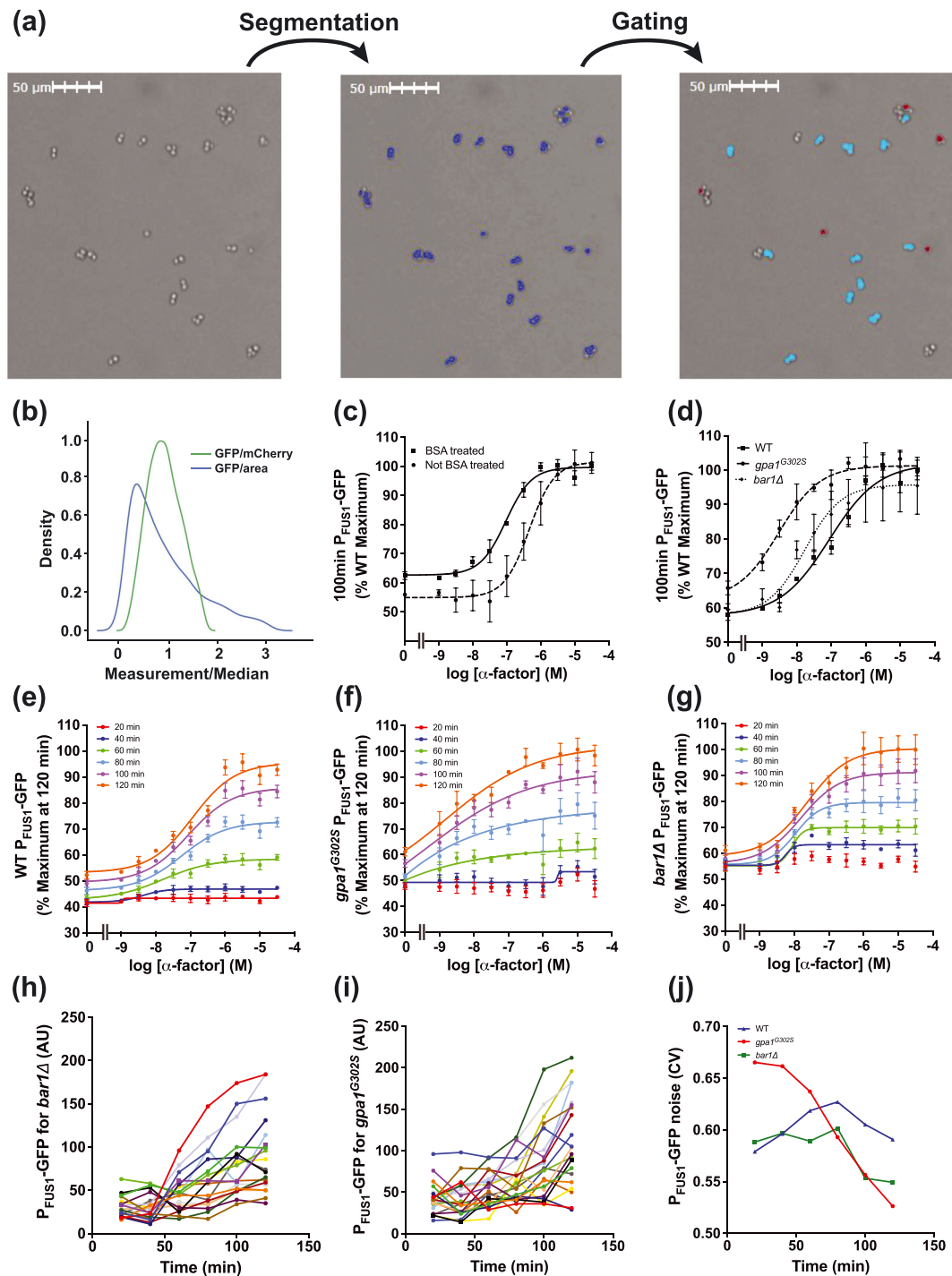


FIGURE 6 Imaging cytometry analysis. Images of the half-area wells of a 96-well plate were captured by the imaging cytometer. (a) The cells were then segmented based on the brightfield image using the Celigo (Nexcelom) native brightfield algorithm and gated based on GFP fluorescence and aspect ratio to identify individual cells. Only singlet cells shown in red in the rightmost panel of (a) were used for single-cell analysis. (b) Distributions of GFP intensity normalized by size and mCherry intensity. (c) Dose-response experiments done with wild-type cells in wells that were either untreated or coated with BSA. (d) Dose-response experiments done with wild-type, *gpa1^{G302S}*, and *bar1Δ* cells in BSA-coated wells. Time courses are shown for (e) wild-type, (f) *gpa1^{G302S}*, and (g) *bar1Δ* cells. Representative single-cell traces of the response to 3 μ M α -factor are shown for (h) wild-type and (i) *gpa1^{G302S}* strains. (j) The cell-to-cell variability is quantified over time for representative traces. Data are presented as mean \pm standard deviation, $N = 3$

for investigating time-dependent changes in the magnitude and cell-to-cell variability in biological processes. To illustrate, we collected single cell traces for wild-type (Figure 6h) and the *gpa1^{G302S}* mutant

(Figure 6i). For each cell, we quantified the GFP intensity and calculated the coefficient of variation (CV) for the population at discrete time points. As compared with wild-type and *bar1Δ*, and as shown

previously, the *gpa1^{G302S}* mutant has higher cell-to-cell variability, but this effect declines with prolonged pheromone stimulation (Figure 6j). The increase in CV was not due to a global increase in gene expression noise, as determined by comparing the normalized mean GFP and mCherry intensities in wild-type and mutant cells. Moreover, the CV in untreated wild-type cells remains relatively constant over time, demonstrating that noise is unaffected by progression through the cell cycle (Dixit et al., 2014). These data illustrate how Sst2 GAP activity acts to suppress cell-to-cell variability following prolonged stimulation with pheromone. Indeed Sst2 is one of a handful of mating pathway components that dampen transcriptional noise in the mating pathway (Colman-Lerner et al., 2005; Dixit et al., 2014; McCullagh et al., 2010). Whereas Sst2 suppresses noise over a broad range of pheromone concentrations (Dixit et al., 2014), Fus3 suppresses noise at high concentrations of pheromone only (Colman-Lerner et al., 2005). Dig1 was reported to suppress noise under basal (unstimulated) conditions (McCullagh et al., 2010).

3.2.4 | Quantification of cell polarization in microfluidics chambers

Most studies of pheromone signalling have been done with uniform and saturating concentrations of ligand. In a physiological setting, however, yeast cells are likely to be exposed to a pheromone gradient coming from a potential mating partner. When that partner is distant, the gradient will be weak and cells (which are nonmotile) will elongate in the direction of the pheromone gradient, thereby increasing the probability of successful mating (Erdman et al., 1998; Hao et al., 2008). In order to identify components and characterize processes required for gradient tracking, we use a custom-built microfluidics chamber capable of producing a linear concentration gradient of pheromone or other stimulus (Dixit et al., 2014; Hao et al., 2008; Kelley et al., 2015). The gradient is achieved by passive diffusion between two parallel microchannels containing standard growth medium or medium with sufficient pheromone to induce cell cycle arrest (Figure S4b,c). With this device, it is also possible to alternate the input channel, or increase or decrease the stimulus concentration, in either a graded or step-wise fashion (Figure S4b). Because there is no direct flow within the growth chamber, cells remain stationary throughout the experiment. Because pheromone is constantly replenished, the effects of Bar1 protease are diminished, and the dose-activity profile is shifted compared to experiments done in tubes or micro-well plates.

Using the microfluidics chamber, we exposed cells to a 0- to 150-nM (wild-type) or 0- to 50-nM (mutant strains) gradient of pheromone. To monitor directionality of growth we used a GFP-tagged variant of Bem1, which binds to activated Cdc42 (Madden & Snyder, 1992). Cdc42-GTP promotes actin polymerization and exocytosis, thereby defining the site of expansion or “polar cap” (Bi & Park, 2012). To assess gradient tracking, we focused on cells residing in the region of the chamber with the largest linear difference in pheromone concentration, as evaluated by the intensity of an inert dye in the pheromone solution. Cell polarization was then monitored over 5-min

intervals. As shown in Figure 7a, cells with a budding (no pheromone) or shmooing (high pheromone) morphology are evident at the boundaries of the chamber. In addition, there is a third morphogenic state, evident at intermediate pheromone concentrations, where cells have stopped dividing but continue to grow in the direction of a weak pheromone gradient (Erdman & Snyder, 2001; Segall, 1993). We refer to this as “elongated” or “chemotropic” growth. After a period of elongated growth, these cells divide once, and the resulting daughter forms a shmoo (Dorer, Pryciak, & Hartwell, 1995; Erdman & Snyder, 2001; Madden & Snyder, 1992; Segall, 1993).

To quantify gradient tracking, we trace the angle of orientation, which is defined as the position of the polar cap relative to the direction of the gradient source, as a function of time. Perfect alignment toward the gradient is defined as zero. As shown in Figure 7b,c, wild-type cells typically exhibit directed growth within 100 minutes, and expansion occurs within ± 45 degrees of the gradient. In cells that express *gpa1^{G302S}*, the polar cap moves along the perimeter of the cell, and the cells expand in an apparently random fashion, as shown previously (Kelley et al., 2015). Kymographs of GFP intensity along the edge of the cell are shown in Figure 7d. The polar cap of wild-type and *bar1 Δ* cells stays in the same location, but the polar cap in *gpa1^{G302S}* cells moves multiple times throughout the duration of the experiment.

To further quantify time-dependent behaviours, we report three other features of cellular morphogenesis: frequency of turning, memory, and persistence (Kelley et al., 2015). Frequency of turning is defined as the frequency of turns greater than 60° . Whereas wild-type cells display large turns less than 1% of the time, cells that express *gpa1^{G302S}* displayed large turns more frequently. Memory is defined as the time period for which the current angle of orientation is correlated with future angles of orientation (autocorrelation). As compared with wild-type, *gpa1^{G302S}* cells spent approximately twice as much time sweeping in any given direction. Finally, persistence is defined as the difference between the position of the polar cap at the beginning and end of a fixed time interval, divided by the total length of the path travelled by the polar cap during that interval. A persistence of 1 corresponds to movement in a straight line, whereas values less than 1 indicate polar cap wandering. By this measure, cells lacking Bar1 or expressing *gpa1^{G302S}* failed to properly track a gradient; the *gpa1^{G302S}* cells in particular displayed half the persistence of that in wild-type cells. The tracking defect exhibited by the *bar1 Δ* cells is well documented (Banderas et al., 2016; Chan & Otte, 1982a; Chen et al., 2016; Ciejek & Thorner, 1979; Diener et al., 2014; Hicks & Herskowitz, 1976; Jackson & Hartwell, 1990a; Jones, Clarke, Craik, & Bennett, 2015; Segota & Franck, 2017). The properties reported here for *gpa1^{G302S}* resemble those reported previously for cells lacking SST2 (Kelley et al., 2015).

Earlier investigations revealed two potential mechanisms by which Sst2 promotes gradient tracking (Dyer et al., 2013; Kelley et al., 2015; McClure et al., 2015). First, Sst2 is required for proper assembly of septins, which form a ring structure at the base of the mating projection that likely serves as a diffusional barrier (Barral, Mermall, Mooseker, & Snyder, 2000; Okada et al., 2013; Takizawa, DeRisi,

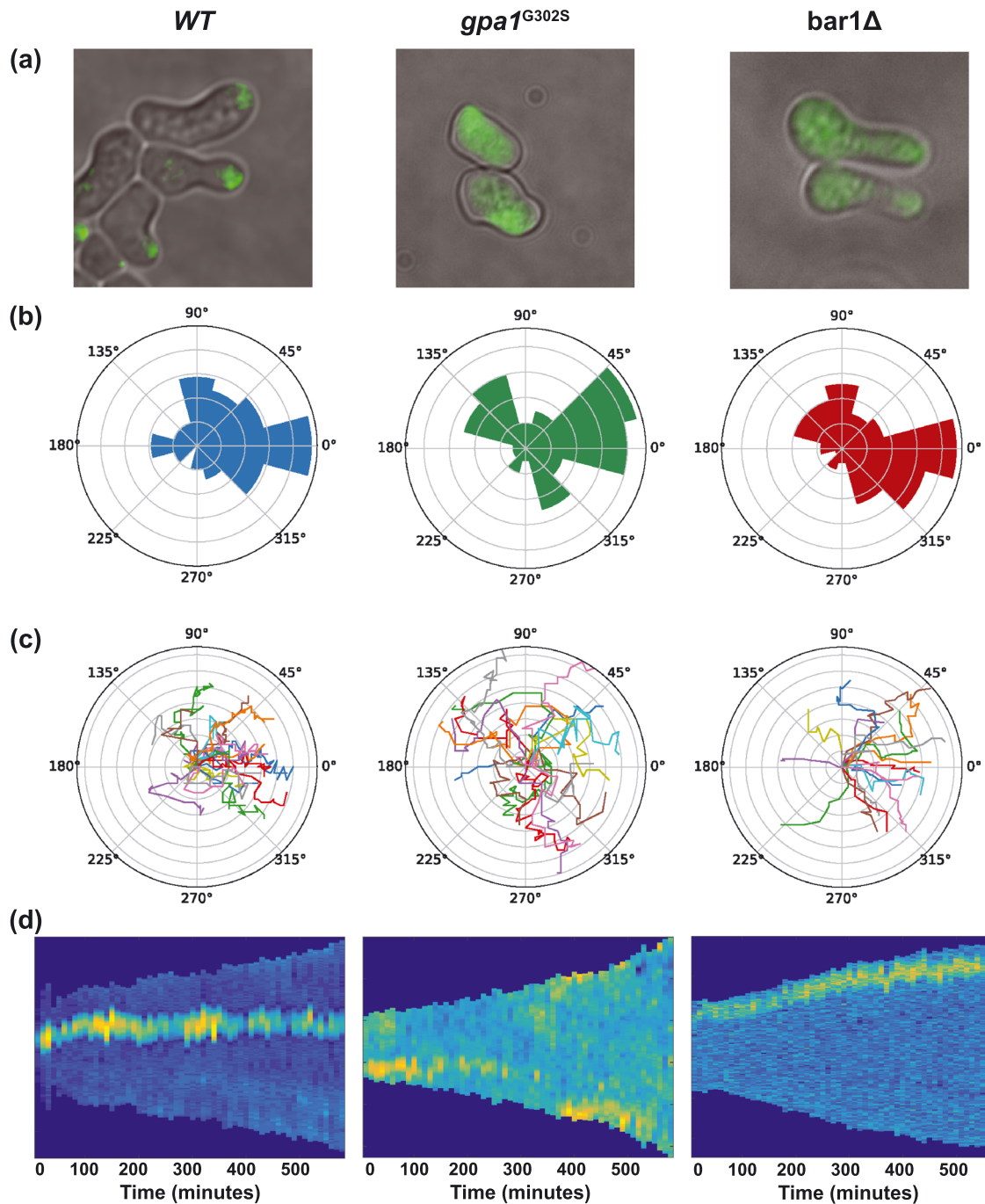


FIGURE 7 Microfluidics for pheromone-induced polarization. Wild-type ($n = 48$), *gpa1^{G302S}* ($n = 47$), and *bar1Δ* ($n = 82$) cells were exposed to a gradient of pheromone. (a) Representative Bem1-GFP fluorescence microscopy images, (b) polar histograms of the angles of the direction of polarized growth, (c) representative single-cell traces of polar caps, and (d) representative kymographs of GFP intensity around the edge of the cell

Wilhelm, & Vale, 2000). In the absence of Sst2, the septin collar is not properly assembled, the polar cap is no longer constrained, and the cell expands in a random direction (Kelley et al., 2015). Second, by virtue of its GAP function, Sst2 abbreviates the lifetime and diffusion of free G $\beta\gamma$ away from the site of receptor activation. In support of this model, G $\beta\gamma$ polarization is needed to prevent polar cap wandering, at least in the presence of a uniform (non-gradient) pheromone stimulus (McClure et al., 2015). The inability to polarize and expand towards

a mating partner may explain why *sst2* mutants mate so poorly despite their increased sensitivity to pheromone.

3.2.5 | Single-cell Fus3 activity assay using time-lapse microscopy

As described above, single-cell analyses of the yeast pheromone pathway have been focused on measuring the transcriptional response. To

directly monitor MAPK activity in single cells, we developed a KTR that is specific for Fus3 activity (Li, Roberts, et al., 2017). The reporter was engineered based on a truncated fragment of a Fus3 substrate, which translocates from the nucleus to the cytoplasm in response to pheromone stimulation. Importantly, this translocation is solely dependent on Fus3-mediated phosphorylation and is unaffected by Kss1. Therefore, nucleocytoplasmic localization changes of the reporter can be used to indicate the kinase activity of Fus3. We have demonstrated that this reporter has a fast response time, full reversibility, a high signal-to-noise ratio, and a high fidelity to Fus3 activity, enabling the real-time tracking of Fus3 signalling in single cells.

To illustrate its applications in studying the pheromone response, we used this reporter to examine the dynamics of Fus3 activity for

wild-type, *bar1Δ* and *gpa1^{G302S}* cells in a microfluidics device (Hao et al., 2013). In response to low (0.3 μM) and high (3 μM) doses of pheromone, we observed a striking difference in Fus3 activation dynamics in wild-type cells. Whereas cells exposed to 3 μM pheromone treatment show a rapid rise in and sustained Fus3 activation, cells exposed to 0.3 μM pheromone exhibit a slow and gradual increase in Fus3 activity (Figure 8a). In contrast, the supersensitive *gpa1^{G302S}* and *bar1Δ* mutants displayed similar responses to 0.3 μM and 3 μM pheromone. Both doses of pheromone induced a sharp increase in Fus3 activity within 10 min, followed by prolonged Fus3 activation (Figure 8b,c). These results indicate that 0.3 μM pheromone is sufficient to saturate the MAPK responses in supersensitive mutants but not in wild-type cells,

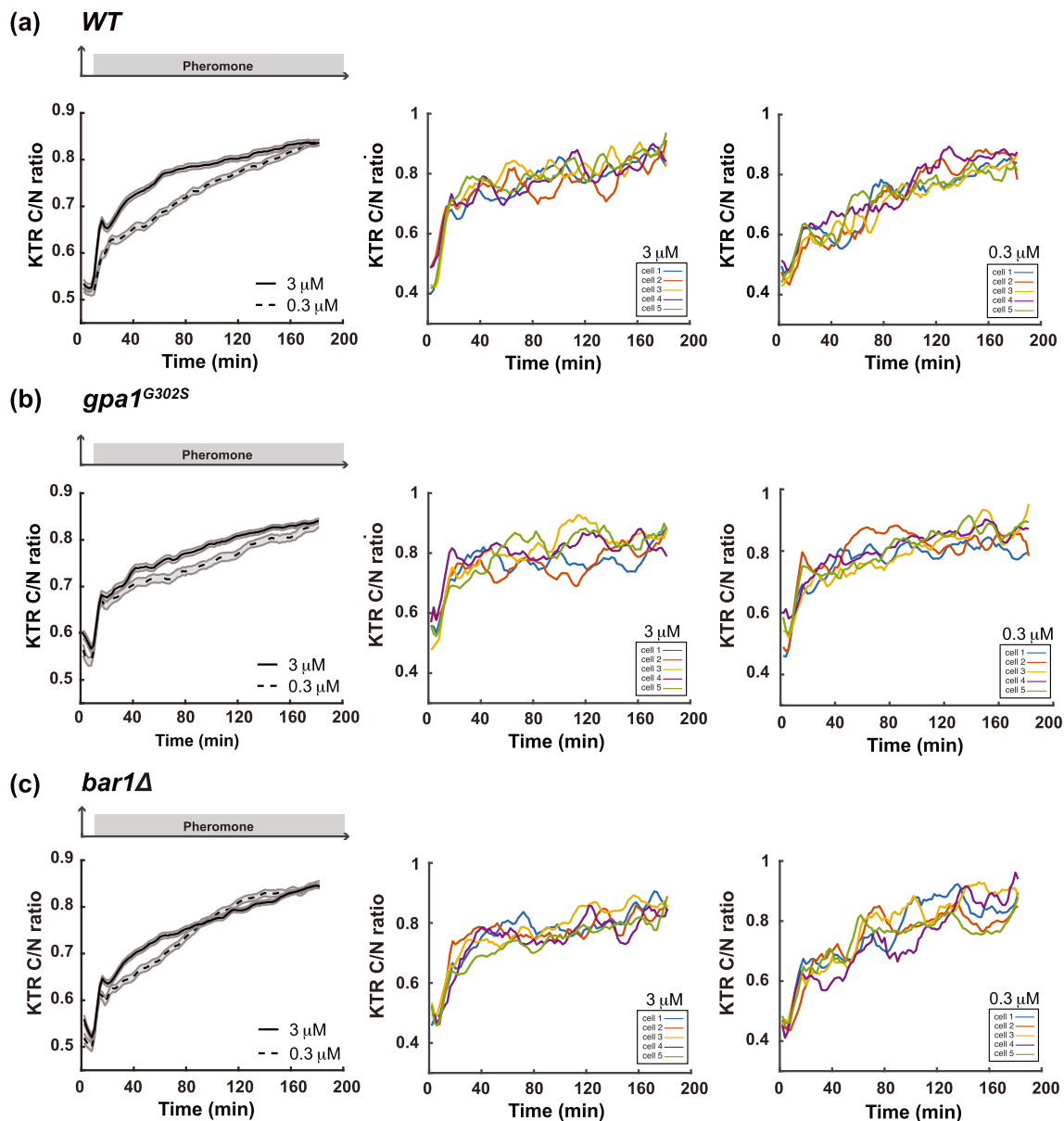


FIGURE 8 Kinase translocation reporter for Fus3 activity. Time traces of reporter responses to 3 μM (solid line) and 0.3 μM pheromone (dashed line) are shown for (a) wild-type, (b) *gpa1^{G302S}*, and (c) *bar1Δ*. Shaded areas represent SE. Representative single cell time traces of Fus3 activation are shown for cells treated with 3 μM and 0.3 μM pheromone. The reporter response was quantified as cytoplasmic over nuclear fluorescence intensities (C/N ratio)

consistent with the results from immunoblotting (Hao et al., 2008; Figure 2).

4 | DISCUSSION

Here, we have compared quantitative measures of MAPK activation, substrate phosphorylation, transcriptional induction, and cell polarization in pheromone-treated cells. For each of these outputs, we presented methods for both population-based as well as single-cell analysis. We illustrated the methods by comparing the activity of wild-type cells with the benchmark *gpa1^{G302S}* and *bar1Δ* supersensitive mutants.

Of the methods described here, MAPK phosphorylation is the most proximal to G protein activation. We have had limited success with two more direct measures of G protein activity, which produce responses that are comparatively weak and transient. One relies on loss of fluorescence resonance energy transfer between fluorescently-tagged Gpa1 and Ste18 (Yi, Kitano, & Simon, 2003). The other quantifies recruitment of overexpressed Ste5 from the nucleus and cytosol to Gβγ at the plasma membrane (Yu, Qi, et al., 2008). We have also not discussed longer-term assays of cell cycle arrest, partner discrimination, and mating efficiency (Jackson & Hartwell, 1990a, 1990b; Sprague, 1991).

Changes in Fus3 or Kss1 phosphorylation are routinely determined by immunoblotting with phospho-p44/42 antibodies. Additionally, these antibodies have been used, in conjunction with fluorescence resonance energy transfer measurements, to document a gradient of activated Fus3 emanating from the shmoo tip into the body of the cell (Maeder et al., 2007). Such spatial regulation of Fus3 may be the result of localized activation (through targeted recruitment of Ste4, Ste20 and Ste5) and global inhibition (by cytoplasmic pools of the MAPK phosphatases Ptp3 and Msg5). However, it is important to note that Fus3 exists in both mono-phosphorylated and dually phosphorylated pools and the phospho-p44/42 antibodies are able to detect, to an extent, both forms of the protein (Bhattacharyya et al., 2006; Hur et al., 2008; Nagiec et al., 2015). This is a potential concern because mono-phosphorylated Fus3 does not stimulate, but rather inhibits, downstream signalling (Nagiec et al., 2015). In contrast, Phos-tag permits the quantitation of dually-phosphorylated, mono-phosphorylated, and non-phosphorylated MAPKs. Thus, we consider the Phos-tag method to be the most informative of the two detection methods. Either method can provide information about the relative sensitivity of various mutants to pheromone however, as illustrated here for the *gpa1^{G302S}* and *bar1Δ* strains.

A major consequence of MAPK activation is new gene transcription. One of the proteins that is induced is Fus3 itself. Thus, Fus3 is part of a positive feedback loop where activation leads to increased expression and a further accumulation of phosphorylated protein. Consequently, there are two schools of thought for what constitutes "MAPK activity." The first argues that the absolute amount or concentration of phosphorylated MAPK dictates pathway output. The second argues that the proportion of protein that is monophosphorylated or

dually phosphorylated is most important. Although we do not attempt to resolve this issue here, data from MAPK activation analysis can be interpreted in light of downstream outputs such as substrate phosphorylation, transcriptional induction, and morphogenesis.

With regard to substrate phosphorylation, a fluorescence-based reporter has recently been developed to specifically monitor Fus3 activity (Li, Roberts, et al., 2017). This reporter is composed of truncated fragments of Fus2, a direct Fus3 substrate. It has been further engineered so that the nucleocytoplasmic localization of this reporter depends solely on Fus3 activation. The reporter exhibits a fast response time, full reversibility, a high signal-to-noise ratio, and a high fidelity for Fus3 over Kss1. Furthermore, as the reporter localizes predominantly in the nucleus before pheromone stimulation, its translocation requires nuclear entry of Fus3 and hence can reflect the dynamic localization of the activated kinase, which is important for inducing appropriate downstream mating responses (Chen, Patterson, Goupil, & Thorner, 2010). As illustrated in Figure 8, this reporter enables time-lapse tracking of Fus3 activity in individual cells in response to pheromone stimulation. Moreover, a substantial number of studies have demonstrated that individual cells respond very differently to the same pheromone treatment (Colman-Lerner et al., 2005; Poritz, Malmstrom, Kim, Rossmessl, & Kamb, 2001; Wang, Hao, Dohlman, & Elston, 2006). This reporter provides a powerful tool to unravel the sources and mechanisms of these cell-to-cell variations and, in particular, the contribution of Fus3 activity to the heterogeneity in the mating response.

For the transcription reporter assays, we compared two common measures of activity: an established method that relies on induction of the enzyme β-galactosidase and a newer method that monitors GFP induction. Based on our comparison (Table 1), the enzymatic assay provides a higher dynamic range than that of the GFP-based assay. This difference may be due in part to the slow maturation time of GFP, which can take up to 45 min (Iizuka, Yamagishi-Shirasaki, & Funatsu, 2011). Another disadvantage of GFP is the potential for confounding effects of changes in cytoplasmic pH. For example, glucose deprivation results in a substantial decrease in intracellular pH, which has been documented to diminish the GFP signal (Isom, Page, Collins, Kopolka, Taghon, & Dohlman, 2018). GFP variants that are less pH-sensitive are available however and may be preferable under some circumstances. Although the β-galactosidase assay provides a superior signal-to-noise readout, its activity is also likely to be affected by chemical perturbants (or genetic mutations). Thus, with either method, careful consideration of experimental controls is needed.

For measurement in individual cells, a GFP (or similar fluorescent protein) reporter is the only option. For this application, we compared single-cell analysis by flow and imaging cytometry. An important advantage of flow cytometry is that these instruments can measure thousands of cells in a single experiment. In addition, some instruments permit the collection of cells with specific light scattering and/or fluorescence characteristics, allowing for the enrichment of mutants with rare signalling or morphological features. Another consideration is the need for a constitutively expressed reference reporter

TABLE 1 Comparison of methods

	Phospho-MAPK antibodies	Phos-tag	β -galactosidase transcriptional reporter	GFP transcriptional reporter	Flow cytometry	Imaging cytometry	Microfluidics	Kinase translocation reporter
MAPK phosphorylation	●	●						
MAPK phosphorylation stoichiometry		●						
MAPK activity	●	●						●
MAPK expression	●	●						
Transcriptional response			●	●	●	●	●	
Morphology						●	●	●
G1 Arrest					●	●	●	●
Gradient tracking							●	
Time-course				●	●	●	●	●
Single-cell					●	●	●	●
Single-cell time-course						●	●	●
High-throughput			●	●	●	●		

Note. All of the methods in this paper have their own advantages and limitations. This table summarizes the capabilities of each method.

to correct for variations in cell size or shape. The use of two reporters requires a flow cytometer than can image multiple fluorescence channels and limits what other fluorophores can be used. Another important limitation of the method is the inability to monitor individual cells over time.

A newer strategy is the use of imaging cytometers. Here we described the use of an automated benchtop instrument (Celigo, Nexelom Biosciences) that provides brightfield and fluorescence imaging of micro-well plates. An important advantage of imaging cytometry over flow cytometry is that a single cell can be tracked over time.

Additionally, some data about cell morphology can be acquired, depending on the resolution of the instrument. Another advantage is the ability to normalize expression to cell size instead of using a second reporter gene (e.g., *P_{ADH1}-mCherry*). A limitation of imaging cytometry is the comparatively small number of cells that can be measured in any given experiment as compared with flow cytometry or population-based assays.

The penultimate step in the mating pathway is polarized cell expansion towards a potential partner. In this regard, an emerging strategy is to use microfluidics chambers to monitor responses to a gradient stimulus. Although cumbersome, it is the only method that can assess the ability of a cell to properly track a gradient over time. This approach can also provide data on cell cycle progression, transcriptional response, and the morphology of individual cells.

The use of microfluidics has uncovered at least two important findings related to pheromone signalling. The first was the realization that Fus3, but not Kss1, is responsible for gradient tracking (Conlon, Gelin-Licht, Ganesan, Zhang, & Levchenko, 2016; Erdman & Snyder, 2001; Errede, Vered, Ford, Pena, & Elston, 2015; Hao et al., 2008; Hegemann et al., 2015; although another group reported a specific requirement for Kss1; Paliwal et al., 2007). This was surprising to us given that Fus3 and Kss1 are both activated by the same upstream protein kinases, and either MAPK can sustain mating transcription and elongated growth (Breitkreutz et al., 2001; Conlon et al., 2016; Erdman & Snyder, 2001; Errede et al., 2015; Hao et al., 2008; Hegemann et al., 2015; Paliwal et al., 2007; Roberts et al., 2000; Zeitlinger et al., 2003). In parallel experiments using phospho-p44/p42 antibodies, we determined that gradient tracking is the result of the distinct temporal and dose-dependent activation properties of Fus3. Whereas Kss1 activation peaks quickly, Fus3 activation increases slowly and at a constant rate that is independent of the pheromone level. Whereas Kss1 is activated with a graded dose-response profile, Fus3 exhibits a steeper dose-response relationship (ultrasensitivity). Using a mutant form of Ste5 that does not bind to Fus3, we determined that Ste5 is necessary for the slow and ultrasensitive activation of Fus3 (Hao et al., 2008; Malleshaiah, Shahrezaei, Swain, & Michnick, 2010). When binding to Ste5 is abrogated, Fus3 activation resembles that of Kss1, and the cell can no longer expand towards a pheromone gradient (Hao et al., 2008). Subsequent work using Phos-tag has revealed a synergistic relationship between two important regulators of Fus3, Ste5 and the dual-specificity phosphatase Msg5 (Nagiec et al., 2015) as well as cooperation between two targets of phosphorylation, Ste5 and the Gy subunit Ste18 (Choudhury, Baradaran-Mashinchi, & Torres, 2018).

Microfluidics studies have also revealed new and important contributions of Sst2. Sst2 is best known as a GTPase-activating protein for Gpa1, but it also binds to the pheromone receptor Ste2 and promotes proper receptor trafficking to the cell surface (Apanovitch, Iiri, Karasawa, Bourne, & Dohlman, 1998; Ballon et al., 2006; Venkatapurapu et al., 2015). Because deletion of Sst2 disrupts both interactions, we have used mutants that uncouple binding to Gpa1 and Ste2 selectively. The *gpa1^{G302S}* mutation prevents binding to Sst2, thereby slowing Gα GTPase activity (DiBello et al., 1998). The

sst2^{Q304N} mutation decreases Sst2 binding to the receptor while leaving RGS-G protein interactions intact (Ballon et al., 2006). Although both mutants are equally supersensitive to pheromone (Dixit et al., 2014), the *gpa1^{G302S}* mutant alone exhibits a defect in polarized cell expansion. These findings point to the GAP activity as essential for gradient tracking.

4.1 | Applications to systems biology

Quantitative measurements of pathway output, at various stimulus concentrations and over broad time scales, have been used to develop mathematical models of the GPCR/MAPK signalling pathway (English et al., 2015; Nagiec et al., 2015). For a detailed review of signal processing and the development of predictive models for MAPK signalling in yeast, we refer the reader to several reviews (Atay & Skotheim, 2017; Hao et al., 2007). In this section, we highlight a few examples from our own work that demonstrate how quantitative measurements and mathematical modelling have been integrated to gain insight into design principles that underlie information processing in these signalling systems. In one case, we used mathematical models to demonstrate how negative regulators of pathway activity play dual roles and promote signalling at specific times during the yeast mating response. In particular, a mathematical model developed in Houser, Ford, Nagiec, Errede, and Elston (2012) was used to explain the counterintuitive observation that deletion of the transcriptional repressor *DIG2* led to a decrease in pheromone-induced transcription, whereas deletion of the homologous gene *DIG1* had the opposite effect (these opposing effects on signal could account for their opposing effects on noise; McCullagh et al., 2010). The model suggested that Dig2 promotes pheromone-induced gene expression by stabilizing the transcriptional activator Ste12. This stabilization creates a large pool of Ste12 that is rapidly activated following exposure to pheromone. These model predictions were then confirmed experimentally using live-cell imaging of a fluorescent reporter for gene expression (Houser et al., 2012).

There is a growing appreciation that cells encode information about environmental conditions not only in the amplitude of pathway activity but also in the temporal response of the signalling network (Purvis & Lahav, 2013). In particular, we used mathematical modelling to demonstrate that information about the stimulus concentration can be encoded in the duration of signal activity (Behar, Hao, Dohlman, & Elston, 2008). This “dose-to-duration” encoding was suggested by quantitative analysis, using mathematical modelling, of experimental data for MAPK signalling during the yeast mating response. Recently, we used quantitative measurements of MAPK signalling to demonstrate that dose-to-duration encoding is also characteristic of MAPK activation in response to high osmolarity signalling (English et al., 2015). Our measurements revealed that the MAPK Hog1 is fully activated in a switch-like fashion over a wide range of salt concentrations, but the duration of MAPK activity is proportional to the salt concentration. Hog1 signalling is thereby converted from a switch to a rheostat, for both phosphorylation of upstream (Ste50) and downstream

(transcription) targets, in a manner that is dependent on the duration of pathway activity (English et al., 2015).

Considerable work has likewise been devoted to modelling polarity establishment and gradient sensing during the yeast pheromone response (Chiou, Balasubramanian, & Lew, 2017). In our own work, we have integrated mathematical modelling with experimental measurements to demonstrate how reshaping of the pheromone gradient through release of the protease Bar1 is used by yeast to avoid competition for potential mating partners (Jin et al., 2011) and to explain the role of polarized G protein activation in tracking pheromone gradients (Kelley et al., 2015; McClure et al., 2015). We have likewise combined quantitative measurements with mathematical modelling to demonstrate how negative feedback in the polarity circuit makes this signaling pathway more robust to variations in the abundance of pathway components (Howell et al., 2012).

Finally, our approach has revealed how Sst2 contributes to proper receptor recovery at the growing edge of pheromone-stimulated cells. In particular, our model predicted that pheromone-induced synthesis of Sst2, coupled with its interaction with the receptor, is required to establish a receptor pool at the polarity site. Again, these results were confirmed by quantitative experimental measurements made using live-cell imaging of fluorescently labelled receptor and with mutants that target the specific functions of Sst2 (Venkatapurapu et al., 2015).

In summary, there is a growing number of examples of how quantitative measurements of pathway activity and noise, at various stimulus concentrations and over broad time scales, have been used to develop mathematical models of GPCR/MAPK signalling in yeast. Such models have been used to identify novel regulatory mechanisms and to predict the behaviour of mutational or environmental perturbations. It is our expectation that the methods and models developed in yeast may eventually be adapted to more complex systems—including humans—to predict the behaviour of genetic, environmental, or pharmacological perturbations affecting human health.

ACKNOWLEDGEMENTS

This work was supported by NIH grants RO1GM111458 (to N. H.), R35GM118105 (to H. G. D.) and RO1GM114136 (to H. G. D. and T. C. E.). The UNC Flow Cytometry Core Facility is supported in part by P30 CA016086 Cancer Center Core Support Grant to the UNC Lineberger Comprehensive Cancer Center.

CONFLICT OF INTEREST

The authors declare that they have no conflict of interest.

AUTHOR CONTRIBUTIONS

J. P. S., A. E. P., Y. L., N. H., and H. G. D. designed the experiments. J. P. S., A. E. P., L. D., and Y. L. performed the experiments. J. P. S., A. E. P., Y. L., N. H., T. E., and H. G. D. wrote the paper. J. P. S. and A. E. P. contributed equally to the paper.

ORCID

Amy E. Pomeroy  <https://orcid.org/0000-0001-9217-3539>

REFERENCES

- AkhavanAghdam, Z., Sinha, J., Tabbaa, O. P., & Hao, N. (2016). Dynamic control of gene regulatory logic by seemingly redundant transcription factors. *eLife*, 5. <http://doi.org/10.7554/eLife.18458>
- Alvaro, C. G., & Thorner, J. (2016). Heterotrimeric G protein-coupled receptor signaling in yeast mating pheromone response. *The Journal of Biological Chemistry*, 291(15), 7788–7795. <http://doi.org/10.1074/jbc.R116.714980>
- Andrews, S. S., Addy, N. J., Brent, R., & Arkin, A. P. (2010). Detailed simulations of cell biology with Smoldyn 2.1. *PLoS Computational Biology*, 6(3), e1000705. <http://doi.org/10.1371/journal.pcbi.1000705>
- Ansel, J., Bottin, H., Rodriguez-Beltran, C., Damon, C., Nagarajan, M., Fehrmann, S., ... Yvert, G. (2008). Cell-to-cell stochastic variation in gene expression is a complex genetic trait. *PLoS Genetics*, 4(4), e1000049. <http://doi.org/10.1371/journal.pgen.1000049>
- Apanovitch, D. M., Iiri, T., Karasawa, T., Bourne, H. R., & Dohlman, H. G. (1998). Second site suppressor mutations of a GTPase-deficient G-protein alpha-subunit. Selective inhibition of Gbeta gamma-mediated signaling. *The Journal of Biological Chemistry*, 273(44), 28597–28602. <https://doi.org/10.1074/jbc.273.44.28597>
- Atay, O., & Skotheim, J. M. (2017). Spatial and temporal signal processing and decision making by MAPK pathways. *The Journal of Cell Biology* <http://doi.org/10.1083/jcb.201609124>JCB, 216, 317–330.
- Ballon, D. R., Flanary, P. L., Gladue, D. P., Konopka, J. B., Dohlman, H. G., & Thorner, J. (2006). DEP-domain-mediated regulation of GPCR signaling responses. *Cell*, 126(6), 1079–1093. <http://doi.org/10.1016/j.cell.2006.07.030>
- Banderas, A., Koltai, M., Anders, A., & Sourjik, V. (2016). Sensory input attenuation allows predictive sexual response in yeast. *Nature Communications*, 7, 12590. <http://doi.org/10.1038/ncomms12590>
- Bao, M. Z., Schwartz, M. A., Cantin, G. T., Yates, J. R., & Madhani, H. D. (2004). Pheromone-dependent destruction of the Tec1 transcription factor is required for MAP kinase signaling specificity in yeast. *Cell*, 119(7), 991–1000. <http://doi.org/10.1016/j.cell.2004.11.052>
- Bardwell, L., Cook, J. G., Zhu-Shimoni, J. X., Voora, D., & Thorner, J. (1998). Differential regulation of transcription: Repression by unactivated mitogen-activated protein kinase Kss1 requires the Dig1 and Dig2 proteins. *Proceedings of the National Academy of Sciences of the United States of America*, 95(26), 15400–15405. <http://doi.org/10.1073/pnas.95.26.15400>
- Barkai, N., Rose, M. D., & Wingreen, N. S. (1998). Protease helps yeast find mating partners. *Nature*, 396(6710), 422–423. <http://doi.org/10.1038/24760>
- Barral, Y., Mermall, V., Mooseker, M. S., & Snyder, M. (2000). Compartmentalization of the cell cortex by septins is required for maintenance of cell polarity in yeast. *Molecular Cell*, 5(5), 841–851. [https://doi.org/10.1016/S1097-2765\(00\)80324-X](https://doi.org/10.1016/S1097-2765(00)80324-X)
- Becskei, A., Kaufmann, B. B., & van Oudenaarden, A. (2005). Contributions of low molecule number and chromosomal positioning to stochastic gene expression. *Nature Genetics*, 37(9), 937–944. <http://doi.org/10.1038/ng1616>
- Behar, M., Hao, N., Dohlman, H. G., & Elston, T. C. (2008). Dose-to-duration encoding and signaling beyond saturation in intracellular signaling networks. *PLoS Computational Biology*, 4(10), e1000197. <http://doi.org/10.1371/journal.pcbi.1000197>
- Bennett, M. R., Pang, W. L., Ostroff, N. A., Baumgartner, B. L., Nayak, S., Tsimring, L. S., & Hasty, J. (2008). Metabolic gene regulation in a dynamically changing environment. *Nature*, 454(7208), 1119–1122. <http://doi.org/10.1038/nature07211>

- Bhattacharyya, R. P., Reményi, A., Good, M. C., Bashor, C. J., Falick, A. M., & Lim, W. A. (2006). The Ste5 scaffold allosterically modulates signaling output of the yeast mating pathway. *Science (New York, N.Y.)*, 311(5762), 822–826. <http://doi.org/10.1126/science.1120941>
- Bi, E., & Park, H.-O. (2012). Cell polarization and cytokinesis in budding yeast. *Genetics*, 191(2), 347–387. <http://doi.org/10.1534/genetics.111.132886>
- Brachmann, C. B., Davies, A., Cost, G. J., Caputo, E., Li, J., Hieter, P., & Boeke, J. D. (1998). Designer deletion strains derived from *Saccharomyces cerevisiae* S288C: A useful set of strains and plasmids for PCR-mediated gene disruption and other applications. *Yeast (Chichester, England)*, 14(2), 115–132. [https://doi.org/10.1002/\(SICI\)1097-0061\(19980130\)14:2<115::AID-YEA204>3.0.CO;2-2](https://doi.org/10.1002/(SICI)1097-0061(19980130)14:2<115::AID-YEA204>3.0.CO;2-2)
- Breitkreutz, A., Boucher, L., & Tyers, M. (2001). MAPK specificity in the yeast pheromone response independent of transcriptional activation. *Current Biology: CB*, 11(16), 1266–1271. [https://doi.org/10.1016/S0960-9822\(01\)00370-0](https://doi.org/10.1016/S0960-9822(01)00370-0)
- Brückner, S., Köhler, T., Braus, G. H., Heise, B., Bolte, M., & Mösch, H.-U. (2004). Differential regulation of Tec1 by Fus3 and Kss1 confers signaling specificity in yeast development. *Current Genetics*, 46(6), 331–342. <http://doi.org/10.1007/s00294-004-0545-1>
- Burkholder, A. C., & Hartwell, L. H. (1985). The yeast alpha-factor receptor: Structural properties deduced from the sequence of the STE2 gene. *Nucleic Acids Research*, 13(23), 8463–8475. <https://doi.org/10.1093/nar/13.23.8463>
- Canagarajah, B. J., Khokhlatchev, A., Cobb, M. H., & Goldsmith, E. J. (1997). Activation mechanism of the MAP kinase ERK2 by dual phosphorylation. *Cell*, 90(5), 859–869. [https://doi.org/10.1016/S0092-8674\(00\)80351-7](https://doi.org/10.1016/S0092-8674(00)80351-7)
- Chan, R. K., & Otte, C. A. (1982a). Isolation and genetic analysis of *Saccharomyces cerevisiae* mutants supersensitive to G1 arrest by a factor and alpha factor pheromones. *Molecular and Cellular Biology*, 2(1), 11–20. <https://doi.org/10.1128/MCB.2.1.11>
- Chan, R. K., & Otte, C. A. (1982b). Physiological characterization of *Saccharomyces cerevisiae* mutants supersensitive to G1 arrest by a factor and alpha factor pheromones. *Molecular and Cellular Biology*, 2(1), 21–29. <https://doi.org/10.1128/MCB.2.1.21>
- Chen, R. E., Patterson, J. C., Goupil, L. S., & Thorner, J. (2010). Dynamic localization of Fus3 mitogen-activated protein kinase is necessary to evoke appropriate responses and avoid cytotoxic effects. *Molecular and Cellular Biology*, 30(17), 4293–4307. <http://doi.org/10.1128/MCB.00361-10>
- Chen, W., Nie, Q., Yi, T.-M., & Chou, C.-S. (2016). Modelling of yeast mating reveals robustness strategies for cell-cell interactions. *PLoS Computational Biology*, 12(7), e1004988. <http://doi.org/10.1371/journal.pcbi.1004988>
- Chiou, J.-G., Balasubramanian, M. K., & Lew, D. J. (2017). Cell polarity in yeast. *Annual Review of Cell and Developmental Biology*, 33, 77–101. <http://doi.org/10.1146/annurev-cellbio-100616-060856>
- Choi, Y. J., Kim, S. K., Kim, S. H., Lee, K. S., & Choi, K. Y. (2000). *Saccharomyces cerevisiae* Ste5 is important for induction and substrate specificity of Fus3 MAP kinase in the pheromone signaling pathway. *Molecules and Cells*, 10(3), 301–308.
- Chou, S., Huang, L., & Liu, H. (2004). Fus3-regulated Tec1 degradation through SCFCdc4 determines MAPK signaling specificity during mating in yeast. *Cell*, 119(7), 981–990. <http://doi.org/10.1016/j.cell.2004.11.053>
- Choudhury, S., Baradaran-Mashinchi, P., & Torres, M. P. (2018). Negative feedback phosphorylation of Gy subunit Ste18 and the Ste5 scaffold synergistically regulates MAPK activation in yeast. *Cell Reports*, 23(5), 1504–1515. <http://doi.org/10.1016/j.celrep.2018.03.135>
- Ciejek, E., & Thorner, J. (1979). Recovery of *S. cerevisiae* a cells from G1 arrest by alpha factor pheromone requires endopeptidase action. *Cell*, 18(3), 623–635. [https://doi.org/10.1016/0092-8674\(79\)90117-X](https://doi.org/10.1016/0092-8674(79)90117-X)
- Colman-Lerner, A., Gordon, A., Serra, E., Chin, T., Resnekov, O., Endy, D., ... Brent, R. (2005). Regulated cell-to-cell variation in a cell-fate decision system. *Nature*, 437(7059), 699–706. <http://doi.org/10.1038/nature03998>
- Conlon, P., Gelin-Licht, R., Ganesan, A., Zhang, J., & Levchenko, A. (2016). Single-cell dynamics and variability of MAPK activity in a yeast differentiation pathway. *Proceedings of the National Academy of Sciences of the United States of America*, 113(40), E5896–E5905. <http://doi.org/10.1073/pnas.1610081113>
- Cook, J. G., Bardwell, L., Kron, S. J., & Thorner, J. (1996). Two novel targets of the MAP kinase Kss1 are negative regulators of invasive growth in the yeast *Saccharomyces cerevisiae*. *Genes & Development*, 10(22), 2831–2848. <http://doi.org/10.1101/gad.10.22.2831>
- Cormack, B. P., Bertram, G., Egerton, M., Gow, N. A., Falkow, S., & Brown, A. J. (1997). Yeast-enhanced green fluorescent protein (yEGFP): A reporter of gene expression in *Candida albicans*. *Microbiology (Reading, England)*, 143(Pt 2), 303–311. <http://doi.org/10.1099/00221287-143-2-303>
- DiBello, P. R., Garrison, T. R., Apanovitch, D. M., Hoffman, G., Shuey, D. J., Mason, K., ... Dohlman, H. G. (1998). Selective uncoupling of RGS action by a single point mutation in the G protein alpha-subunit. *The Journal of Biological Chemistry*, 273(10), 5780–5784. <https://doi.org/10.1074/jbc.273.10.5780>
- Diener, C., Schreiber, G., Giese, W., del Rio, G., Schröder, A., & Klipp, E. (2014). Yeast mating and image-based quantification of spatial pattern formation. *PLoS Computational Biology*, 10(6), e1003690. <http://doi.org/10.1371/journal.pcbi.1003690>
- Dixit, G., Kelley, J. B., Houser, J. R., Elston, T. C., & Dohlman, H. G. (2014). Cellular noise suppression by the regulator of G protein signaling Sst2. *Molecular Cell*, 55(1), 85–96. <http://doi.org/10.1016/j.molcel.2014.05.019>
- Dong, S., Rogan, S. C., & Roth, B. L. (2010). Directed molecular evolution of DREADDs: A generic approach to creating next-generation RASSLs. *Nature Protocols*, 5(3), 561–573. <http://doi.org/10.1038/nprot.2009.239>
- Dorer, R., Pryciak, P. M., & Hartwell, L. H. (1995). *Saccharomyces cerevisiae* cells execute a default pathway to select a mate in the absence of pheromone gradients. *The Journal of Cell Biology*, 131(4), 845–861. <https://doi.org/10.1083/jcb.131.4.845>
- Dowell, S. J., & Brown, A. J. (2009). Yeast assays for G protein-coupled receptors. *Methods in Molecular Biology (Clifton, N.J.)*, 552, 213–229. http://doi.org/10.1007/978-1-60327-317-6_15
- Dyer, J. M., Savage, N. S., Jin, M., Zyla, T. R., Elston, T. C., & Lew, D. J. (2013). Tracking shallow chemical gradients by actin-driven wandering of the polarization site. *Current Biology: CB*, 23(1), 32–41. <http://doi.org/10.1016/j.cub.2012.11.014>
- Elion, E. A., Grisafi, P. L., & Fink, G. R. (1990). FUS3 encodes a cdc2+/CDC28-related kinase required for the transition from mitosis into conjugation. *Cell*, 60(4), 649–664. [https://doi.org/10.1016/0092-8674\(90\)90668-5](https://doi.org/10.1016/0092-8674(90)90668-5)
- Elion, E. A., Satterberg, B., & Kranz, J. E. (1993). FUS3 phosphorylates multiple components of the mating signal transduction cascade: Evidence for STE12 and FAR1. *Molecular Biology of the Cell*, 4(5), 495–510. <https://doi.org/10.1091/mbc.4.5.495>
- Elowitz, M. B., Levine, A. J., Siggia, E. D., & Swain, P. S. (2002). Stochastic gene expression in a single cell. *Science (New York, N.Y.)*, 297(5584), 1183–1186. <http://doi.org/10.1126/science.1070919>
- English, J. G., Shellhammer, J. P., Malahe, M., McCarter, P. C., Elston, T. C., & Dohlman, H. G. (2015). MAPK feedback encodes a switch and timer

- for tunable stress adaptation in yeast. *Science Signaling*, 8(359), ra5. <http://doi.org/10.1126/scisignal.2005774>
- Erdman, S., Lin, L., Malczynski, M., & Snyder, M. (1998). Pheromone-regulated genes required for yeast mating differentiation. *The Journal of Cell Biology*, 140(3), 461–483. <https://doi.org/10.1083/jcb.140.3.461>
- Erdman, S., & Snyder, M. (2001). A filamentous growth response mediated by the yeast mating pathway. *Genetics*, 159(3), 919–928.
- Errede, B., Vered, L., Ford, E., Pena, M. I., & Elston, T. C. (2015). Pheromone-induced morphogenesis and gradient tracking are dependent on the MAPK Fus3 binding to Ga. *Molecular Biology of the Cell*, 26(18), 3343–3358. <http://doi.org/10.1091/mbc.E15-03-0176>
- Ferrell, J. E., & Bhatt, R. R. (1997). Mechanistic studies of the dual phosphorylation of mitogen-activated protein kinase. *The Journal of Biological Chemistry*, 272(30), 19008–19016. <https://doi.org/10.1074/jbc.272.30.19008>
- Fraser, H. B., Hirsh, A. E., Giaever, G., Kumm, J., & Eisen, M. B. (2004). Noise minimization in eukaryotic gene expression. *PLoS Biology*, 2(6), e137. <http://doi.org/10.1371/journal.pbio.0020137>
- Friedman, J., & Yurtsev, E. (2017). FlowCytometryTools. <http://doi.org/10.5281/zenodo.32991>
- Gelperin, D. M., White, M. A., Wilkinson, M. L., Kon, Y., Kung, L. A., Wise, K. J., ... Grayhack, E. J. (2005). Biochemical and genetic analysis of the yeast proteome with a movable ORF collection. *Genes & Development*, 19(23), 2816–2826. <http://doi.org/10.1101/gad.1362105>
- Ghaemmaghami, S., Huh, W.-K., Bower, K., Howson, R. W., Belle, A., Dephoure, N., ... Weissman, J. S. (2003). Global analysis of protein expression in yeast. *Nature*, 425(6959), 737–741. <http://doi.org/10.1038/nature02046>
- Gietz, R. D., & Woods, R. A. (2002). Transformation of yeast by lithium acetate/single-stranded carrier DNA/polyethylene glycol method. *Methods in Enzymology*, 350, 87–96. [https://doi.org/10.1016/S0076-6879\(02\)50957-5](https://doi.org/10.1016/S0076-6879(02)50957-5)
- Hagen, D. C., McCaffrey, G., & Sprague, G. F. (1991). Pheromone response elements are necessary and sufficient for basal and pheromone-induced transcription of the FUS1 gene of *Saccharomyces cerevisiae*. *Molecular and Cellular Biology*, 11(6), 2952–2961. <https://doi.org/10.1128/MCB.11.6.2952>
- Hansen, A. S., Hao, N., & O'Shea, E. K. (2015). High-throughput microfluidics to control and measure signaling dynamics in single yeast cells. *Nature Protocols*, 10(8), 1181–1197. <http://doi.org/10.1038/nprot.2015.079>
- Hao, N., Behar, M., Elston, T. C., & Dohlman, H. G. (2007). Systems biology analysis of G protein and MAP kinase signaling in yeast. *Oncogene*, 26(22), 3254–3266. <http://doi.org/10.1038/sj.onc.1210416>
- Hao, N., Budnik, B. A., Gunawardena, J., & O'Shea, E. K. (2013). Tunable signal processing through modular control of transcription factor translocation. *Science (New York, N.Y.)*, 339(6118), 460–464. <http://doi.org/10.1126/science.1227299>
- Hao, N., Nayak, S., Behar, M., Shanks, R. H., Nagiec, M. J., Hasty, J., ... Dohlman, H. G. (2008). Regulation of cell signalling dynamics by the protein kinase-scaffold Ste5. *Molecular Cell*, 30(5), 649–656. <http://doi.org/10.1016/j.molcel.2008.04.016>
- Hao, N., & O'Shea, E. K. (2011). Signal-dependent dynamics of transcription factor translocation controls gene expression. *Nature Structural & Molecular Biology*, 19(1), 31–39. <http://doi.org/10.1038/nsmb.2192>
- Haystead, T. A. J., Dent, P., Wu, J., Haystead, C. M. M., & Sturgill, T. W. (1992). Ordered phosphorylation of p42 mapk by MAP kinase kinase. *FEBS Letters*, 306(1), 17–22. [http://doi.org/10.1016/0014-5793\(92\)80828-5](http://doi.org/10.1016/0014-5793(92)80828-5)
- Hegemann, B., Unger, M., Lee, S. S., Stoffel-Studer, I., van den Heuvel, J., Pelet, S., ... Peter, M. (2015). A cellular system for spatial signal decoding in chemical gradients. *Developmental Cell*, 35(4), 458–470. <http://doi.org/10.1016/j.devcel.2015.10.013>
- Hicks, J. B., & Herskowitz, I. (1976). Evidence for a new diffusible element of mating pheromones in yeast. *Nature*, 260(5548), 246–248. <https://doi.org/10.1038/260246a0>
- Hoffman, G. A., Garrison, T. R., & Dohlman, H. G. (2000). Endoproteolytic processing of Sst2, a multidomain regulator of G protein signaling in yeast. *The Journal of Biological Chemistry*, 275(48), 37533–37541. <http://doi.org/10.1074/jbc.M005751200>
- Hoffman, G. A., Garrison, T. R., & Dohlman, H. G. (2002). Analysis of RGS proteins in *Saccharomyces cerevisiae*. *Methods in Enzymology*, 344, 617–631. [https://doi.org/10.1016/S0076-6879\(02\)44744-1](https://doi.org/10.1016/S0076-6879(02)44744-1)
- Houser, J. R., Ford, E., Nagiec, M. J., Errede, B., & Elston, T. C. (2012). Positive roles for negative regulators in the mating response of yeast. *Molecular Systems Biology*, 8(586), 1–10. <http://doi.org/10.1038/msb.2012.18>
- Howell, A. S., Jin, M., Wu, C.-F., Zyla, T. R., Elston, T. C., & Lew, D. J. (2012). Negative feedback enhances robustness in the yeast polarity establishment circuit. *Cell*, 149(2), 322–333. <http://doi.org/10.1016/j.cell.2012.03.012>
- Huh, W.-K., Falvo, J. V., Gerke, L. C., Carroll, A. S., Howson, R. W., Weissman, J. S., & O'Shea, E. K. (2003). Global analysis of protein localization in budding yeast. *Nature*, 425, 686–691. <https://doi.org/10.1038/nature02026>
- Hung, W., Olson, K. A., Breitkreutz, A., & Sadowski, I. (1997). Characterization of the basal and pheromone-stimulated phosphorylation states of Ste12p. *European Journal of Biochemistry*, 245(2), 241–251. <https://doi.org/10.1111/j.1432-1033.1997.00241.x>
- Hur, J.-Y., Kang, G.-Y., Choi, M.-Y., Jung, J. W., Kim, K.-P., & Park, S.-H. (2008). Quantitative profiling of dual phosphorylation of Fus3 MAP kinase in *Saccharomyces cerevisiae*. *Molecules and Cells*, 26(1), 41–47.
- Hutter, K. J., & Eipel, H. E. (1978). Flow cytometric determinations of cellular substances in algae, bacteria, moulds and yeasts. *Antonie Van Leeuwenhoek*, 44(3–4), 269–282. <https://doi.org/10.1007/BF00394305>
- Iizuka, R., Yamagishi-Shirasaki, M., & Funatsu, T. (2011). Kinetic study of de novo chromophore maturation of fluorescent proteins. *Analytical Biochemistry*, 414(2), 173–178. <http://doi.org/10.1016/j.ab.2011.03.036>
- Isom, D. G., Page, S. C., Collins, L. B., Kapolka, N. J., Taghon, G. J., & Dohlman, H. G. (2018). Coordinated regulation of intracellular pH by two glucose-sensing pathways in yeast. *The Journal of Biological Chemistry*, 293(7), 2318–2329. <http://doi.org/10.1074/jbc.RA117.000422>
- Jackson, C. L., & Hartwell, L. H. (1990a). Courtship in *S. cerevisiae*: Both cell types choose mating partners by responding to the strongest pheromone signal. *Cell*, 63(5), 1039–1051. [https://doi.org/10.1016/0092-8674\(90\)90507-B](https://doi.org/10.1016/0092-8674(90)90507-B)
- Jackson, C. L., & Hartwell, L. H. (1990b). Courtship in *Saccharomyces cerevisiae*: An early cell-cell interaction during mating. *Molecular and Cellular Biology*, 10(5), 2202–2213. <https://doi.org/10.1128/MCB.10.5.2202>
- Janes, K. A. (2015). An analysis of critical factors for quantitative immunoblotting. *Science Signaling*, 8(371), rs2. <http://doi.org/10.1126/scisignal.2005966>
- Janke, C., Magiera, M. M., Rathfelder, N., Taxis, C., Reber, S., Maekawa, H., ... Knop, M. (2004). A versatile toolbox for PCR-based tagging of yeast genes: New fluorescent proteins, more markers and promoter substitution cassettes. *Yeast (Chichester, England)*, 21(11), 947–962. <http://doi.org/10.1002/yea.1142>
- Jiang, Y., AkhavanAghdam, Z., Tsimring, L. S., & Hao, N. (2017). Coupled feedback loops control the stimulus-dependent dynamics of the yeast

- transcription factor Msn2. *Journal of Biological Chemistry*, 292(30), 12366–12372. <http://doi.org/10.1074/jbc.C117.800896>
- Jin, M., Errede, B., Behar, M., Mather, W., Nayak, S., Hastly, J., ... Elston, T. C. (2011). Yeast dynamically modify their environment to achieve better mating efficiency. *Science Signaling*, 4(186), ra54. <http://doi.org/10.1126/scisignal.2001763>
- Jones, S. K., Clarke, S. C., Craik, C. S., & Bennett, R. J. (2015). Evolutionary selection on barrier activity: Bar1 is an aspartyl protease with novel substrate specificity. *MBio*, 6(6), e01604–e01615. <http://doi.org/10.1128/mBio.01604-15>
- Kelley, J. B., Dixit, G., Sheetz, J. B., Venkatapurapu, S. P., Elston, T. C., & Dohlman, H. G. (2015). RGS proteins and septins cooperate to promote chemotropism by regulating polar cap mobility. *Current Biology: CB*, 25(3), 275–285. <http://doi.org/10.1016/j.cub.2014.11.047>
- Kinoshita, E., Kinoshita-Kikuta, E., Takiyama, K., & Koike, T. (2006). Phosphate-binding tag, a new tool to visualize phosphorylated proteins. *Molecular & Cellular Proteomics: MCP*, 5(4), 749–757. <http://doi.org/10.1074/mcp.T500024-MCP200>
- Kinoshita-Kikuta, E., Aoki, Y., Kinoshita, E., & Koike, T. (2007). Label-free kinase profiling using phosphate affinity polyacrylamide gel electrophoresis. *Molecular & Cellular Proteomics: MCP*, 6(2), 356–366. <http://doi.org/10.1074/mcp.T600044-MCP200>
- Lambert, N. A., Johnston, C. A., Cappell, S. D., Kuravi, S., Kimple, A. J., Willard, F. S., & Siderovski, D. P. (2010). Regulators of G-protein signaling accelerate GPCR signaling kinetics and govern sensitivity solely by accelerating GTPase activity. *Proceedings of the National Academy of Sciences*, 107(15), 7066–7071. <http://doi.org/10.1073/pnas.0912934107>
- Lee, M. J., & Dohlman, H. G. (2008). Coactivation of G protein signaling by cell-surface receptors and an intracellular exchange factor. *Current Biology*, 18(3), 211–215. <http://doi.org/10.1016/j.cub.2008.01.007>
- Li, Y., Jin, M., O'Laughlin, R., Bittihn, P., Tsimring, L. S., Pillus, L., ... Hao, N. (2017). Multigenerational silencing dynamics control cell aging. *Proceedings of the National Academy of Sciences*, 114(42), 11253–11258. <http://doi.org/10.1073/pnas.1703379114>
- Li, Y., Roberts, J., AkhavanAghdam, Z., & Hao, N. (2017). Mitogen-activated protein kinase (MAPK) dynamics determine cell fate in the yeast mating response. *The Journal of Biological Chemistry*, 292(50), 20354–20361. <http://doi.org/10.1074/jbc.AC117.000548>
- MacKay, V. L., Armstrong, J., Yip, C., Welch, S., Walker, K., Osborn, S., ... Forstrom, J. (1991). Characterization of the Bar proteinase, an extracellular enzyme from the yeast *Saccharomyces cerevisiae*. *Advances in Experimental Medicine and Biology*, 306, 161–172. https://doi.org/10.1007/978-1-4684-6012-4_21
- Madden, K., & Snyder, M. (1992). Specification of sites for polarized growth in *Saccharomyces cerevisiae* and the influence of external factors on site selection. *Molecular Biology of the Cell*, 3(9), 1025–1035. <http://doi.org/10.1091/mbc.3.9.1025>
- Madhani, H. D., Galitski, T., Lander, E. S., & Fink, G. R. (1999). Effectors of a developmental mitogen-activated protein kinase cascade revealed by expression signatures of signaling mutants. *Proceedings of the National Academy of Sciences of the United States of America*, 96(22), 12530–12535. <https://doi.org/10.1073/pnas.96.22.12530>
- Maeder, C. I., Hink, M. A., Kinkhabwala, A., Mayr, R., Bastiaens, P. I. H., & Knop, M. (2007). Spatial regulation of Fus3 MAP kinase activity through a reaction-diffusion mechanism in yeast pheromone signalling. *Nature Cell Biology*, 9(11), 1319–1326. <http://doi.org/10.1038/ncb1652>
- Malleshaiah, M. K., Shahrezaei, V., Swain, P. S., & Michnick, S. W. (2010). The scaffold protein Ste5 directly controls a switch-like mating decision in yeast. *Nature*, 465(7294), 101–105. <http://doi.org/10.1038/nature08946>
- Martzen, M. R., McCraith, S. M., Spinelli, S. L., Torres, F. M., Fields, S., Grayhack, E. J., & Phizicky, E. M. (1999). A biochemical genomics approach for identifying genes by the activity of their products. *Science (New York, N.Y.)*, 286(5442), 1153–1155. <https://doi.org/10.1126/science.286.5442.1153>
- McAdams, H. H., & Arkin, A. (1999). It's a noisy business! Genetic regulation at the nanomolar scale. *Trends in Genetics: TIG*, 15(2), 65–69. [https://doi.org/10.1016/S0168-9525\(98\)01659-X](https://doi.org/10.1016/S0168-9525(98)01659-X)
- McCaffrey, G., Clay, F. J., Kelsay, K., & Sprague, G. F. (1987). Identification and regulation of a gene required for cell fusion during mating of the yeast *Saccharomyces cerevisiae*. *Molecular and Cellular Biology*, 7(8), 2680–2690. <https://doi.org/10.1128/MCB.7.8.2680>
- McClure, A. W., Minakova, M., Dyer, J. M., Zyla, T. R., Elston, T. C., & Lew, D. J. (2015). Role of polarized G protein signaling in tracking pheromone gradients. *Developmental Cell*, 35(4), 471–482. <http://doi.org/10.1016/j.devcel.2015.10.024>
- McCullagh, E., Seshan, A., El-Samad, H., & Madhani, H. D. (2010). Coordinate control of gene expression noise and interchromosomal interactions in a MAP kinase pathway. *Nature Cell Biology*, 12(10), 954–962. <http://doi.org/10.1038/ncb2097>
- Mentesana, P. E., Dossil, M., & Konopka, J. B. (2002). Functional assays for mammalian G-protein-coupled receptors in yeast. *Methods in Enzymology*, 344, 92–111. [https://doi.org/10.1016/S0076-6879\(02\)44708-8](https://doi.org/10.1016/S0076-6879(02)44708-8)
- Minic, J., Persuy, M.-A., Godel, E., Aioun, J., Connerton, I., Salesse, R., & Pajot-Augy, E. (2005). Functional expression of olfactory receptors in yeast and development of a bioassay for odorant screening. *The FEBS Journal*, 272(2), 524–537. <http://doi.org/10.1111/j.1742-4658.2004.04494.x>
- Minic, J., Sautel, M., Salesse, R., & Pajot-Augy, E. (2005). Yeast system as a screening tool for pharmacological assessment of G protein coupled receptors. *Current Medicinal Chemistry*, 12(8), 961–969. <https://doi.org/10.2174/0929867053507261>
- Moore, T. I., Chou, C.-S., Nie, Q., Jeon, N. L., & Yi, T.-M. (2008). Robust spatial sensing of mating pheromone gradients by yeast cells. *PLoS ONE*, 3(12), e3865. <http://doi.org/10.1371/journal.pone.0003865>
- Moore, T. I., Tanaka, H., Kim, H. J., Jeon, N. L., & Yi, T.-M. (2013). Yeast G-proteins mediate directional sensing and polarization behaviors in response to changes in pheromone gradient direction. *Molecular Biology of the Cell*, 24(4), 521–534. <http://doi.org/10.1091/mbc.e12-10-0739>
- Nagiec, M. J., McCarter, P. C., Kelley, J. B., Dixit, G., Elston, T. C., & Dohlman, H. G. (2015). Signal inhibition by a dynamically regulated pool of monophosphorylated MAPK. *Molecular Biology of the Cell*, 26(18), 3359–3371. <http://doi.org/10.1091/mbc.E15-01-0037>
- Okada, S., Leda, M., Hanna, J., Savage, N. S., Bi, E., & Goryachev, A. B. (2013). Daughter cell identity emerges from the interplay of Cdc42, septins, and exocytosis. *Developmental Cell*, 26(2), 148–161. <http://doi.org/10.1016/j.devcel.2013.06.015>
- Paliwal, S., Iglesias, P. A., Campbell, K., Hilioti, Z., Groisman, A., & Levchenko, A. (2007). MAPK-mediated bimodal gene expression and adaptive gradient sensing in yeast. *Nature*, 446(7131), 46–51. <http://doi.org/10.1038/nature05561>
- Pei, Y., Dong, S., & Roth, B. L. (2010). Generation of designer receptors exclusively activated by designer drugs (DREADDs) using directed molecular evolution. *Current Protocols in Neuroscience*, Chapter 4, Unit 4, 33. <http://doi.org/10.1002/0471142301.ns0433s50>
- Pesce, C. G., Zdraljevic, S., Peria, W. J., Bush, A., Repetto, M. V., Rockwell, D., ... Brent, R. (2018). Single-cell profiling screen identifies microtubule-dependent reduction of variability in signaling. *Molecular Systems Biology*, 14(4), e7390. <http://doi.org/10.15252/msb.20167390>

- Pope, P. A., & Pryciak, P. M. (2013). Functional overlap among distinct G1/S inhibitory pathways allows robust G1 arrest by yeast mating pheromones. *Molecular Biology of the Cell*, 24(23), 3675–3688. <http://doi.org/10.1091/mbc.E13-07-0373>
- Poritz, M. A., Malmstrom, S., Kim, M. K., Rossmeissl, P. J., & Kamb, A. (2001). Graded mode of transcriptional induction in yeast pheromone signalling revealed by single-cell analysis. *Yeast (Chichester, England)*, 18(14), 1331–1338. <http://doi.org/10.1002/yea.777>
- Purvis, J. E., & Lahav, G. (2013). Encoding and decoding cellular information through signaling dynamics. *Cell*, 152(5), 945–956. <http://doi.org/10.1016/j.cell.2013.02.005>
- Raser, J. M., & O'Shea, E. K. (2004). Control of stochasticity in eukaryotic gene expression. *Science (New York, N.Y.)*, 304(5678), 1811–1814. <http://doi.org/10.1126/science.1098641>
- Roberts, C. J., Nelson, B., Marton, M. J., Stoughton, R., Meyer, M. R., Bennett, H. A., ... Friend, S. H. (2000). Signaling and circuitry of multiple MAPK pathways revealed by a matrix of global gene expression profiles. *Science*, 287(5454), 873–880. <https://doi.org/10.1126/science.287.5454.873>
- Sabbagh, W., Flatauer, L. J., Bardwell, A. J., & Bardwell, L. (2001). Specificity of MAP kinase signaling in yeast differentiation involves transient versus sustained MAPK activation. *Molecular Cell*, 8(3), 683–691. [https://doi.org/10.1016/S1097-2765\(01\)00322-7](https://doi.org/10.1016/S1097-2765(01)00322-7)
- Schneider, C. A., Rasband, W. S., & Eliceiri, K. W. (2012). NIH Image to ImageJ: 25 years of image analysis. *Nature Methods*, 9(7), 671–675. <https://doi.org/10.1038/nmeth.2089>
- Segall, J. E. (1993). Polarization of yeast cells in spatial gradients of alpha mating factor. *Proceedings of the National Academy of Sciences of the United States of America*, 90(18), 8332–8336. <https://doi.org/10.1073/pnas.90.18.8332>
- Segota, I., & Franck, C. (2017). Extracellular processing of molecular gradients by eukaryotic cells can improve gradient detection accuracy. *Physical Review Letters*, 119(24), 248101. <http://doi.org/10.1103/PhysRevLett.119.248101>
- Shellhammer, J. P., Morin-Kensicki, E., Matson, J. P., Yin, G., Isom, D. G., Campbell, S. L., ... Dohlman, H. G. (2017). Amino acid metabolites that regulate G protein signaling during osmotic stress. *PLoS Genetics*, 13(5), e1006829. <https://doi.org/10.1371/journal.pgen.1006829>
- Siekhaus, D. E., & Drubin, D. G. (2003). Spontaneous receptor-independent heterotrimeric G-protein signalling in an RGS mutant. *Nature Cell Biology*, 5(3), 231–235. <http://doi.org/10.1038/ncb941>
- Sikorski, R. S., & Hieter, P. (1989). A system of shuttle vectors and yeast host strains designed for efficient manipulation of DNA in *Saccharomyces cerevisiae*. *Genetics*, 122(1), 19–27.
- Song, D., Dolan, J. W., Yuan, Y. L., & Fields, S. (1991). Pheromone-dependent phosphorylation of the yeast STE12 protein correlates with transcriptional activation. *Genes & Development*, 5(5), 741–750. <https://doi.org/10.1101/gad.5.5.741>
- Sprague, G. F. (1991). Assay of yeast mating reaction. *Methods in Enzymology*, 194, 77–93. [https://doi.org/10.1016/0076-6879\(91\)94008-Z](https://doi.org/10.1016/0076-6879(91)94008-Z)
- Takizawa, P. A., DeRisi, J. L., Wilhelm, J. E., & Vale, R. D. (2000). Plasma membrane compartmentalization in yeast by messenger RNA transport and a septin diffusion barrier. *Science (New York, N.Y.)*, 290(5490), 341–344. <https://doi.org/10.1126/science.290.5490.341>
- Tedford, K., Kim, S., Sa, D., Stevens, K., & Tyers, M. (1997). Regulation of the mating pheromone and invasive growth responses in yeast by two MAP kinase substrates. *Current Biology*, 7(4), 228–238. [http://doi.org/10.1016/S0960-9822\(06\)00118-7](http://doi.org/10.1016/S0960-9822(06)00118-7)
- Trueheart, J., Boeke, J. D., & Fink, G. R. (1987). Two genes required for cell fusion during yeast conjugation: Evidence for a pheromone-induced surface protein. *Molecular and Cellular Biology*, 7(7), 2316–2328. <http://doi.org/10.1128/MCB.7.7.2316>. Updated
- Venkatapurapu, S. P., Kelley, J. B., Dixit, G., Pena, M., Errede, B., Dohlman, H. G., & Elston, T. C. (2015). Modulation of receptor dynamics by the regulator of G protein signaling Sst2. *Molecular Biology of the Cell*, 26(22), 4124–4134. <http://doi.org/10.1091/mbc.E14-12-1635>
- Volfson, D., Marciniak, J., Blake, W. J., Ostroff, N., Tsimring, L. S., & Hasty, J. (2006). Origins of extrinsic variability in eukaryotic gene expression. *Nature*, 439(7078), 861–864. <http://doi.org/10.1038/nature04281>
- Wach, A., Brachat, A., Pöhlmann, R., & Philippsen, P. (1994). New heterologous modules for classical or PCR-based gene disruptions in *Saccharomyces cerevisiae*. *Yeast (Chichester, England)*, 10(13), 1793–1808. <https://doi.org/10.1002/yea.320101310>
- Wang, X., Hao, N., Dohlman, H. G., & Elston, T. C. (2006). Bistability, stochasticity, and oscillations in the mitogen-activated protein kinase cascade. *Biophysical Journal*, 90(6), 1961–1978. <http://doi.org/10.1529/biophysj.105.073874>
- Wang, Y., & Dohlman, H. G. (2004). Pheromone signaling mechanisms in yeast: A prototypical sex machine. *Science (New York, N.Y.)*, 306(5701), 1508–1509. <http://doi.org/10.1126/science.1104568>
- Winters, M. J., & Pryciak, P. M. (2018). Analysis of the thresholds for transcriptional activation by the yeast MAP kinases Fus3 and Kss1. *Molecular Biology of the Cell*, 29(5), 669–682. <http://doi.org/10.1091/mbc.E17-10-0578>
- Winzeler, E. A., Shoemaker, D. D., Astromoff, A., Liang, H., Anderson, K., Andre, B., ... Davis, R. W. (1999). Functional characterization of the *S. cerevisiae* genome by gene deletion and parallel analysis. *Science (New York, N.Y.)*, 285(5429), 901–906. <https://doi.org/10.1126/science.285.5429.901>
- Yi, T.-M., Kitano, H., & Simon, M. I. (2003). A quantitative characterization of the yeast heterotrimeric G protein cycle. *Proceedings of the National Academy of Sciences*, 100(19), 10764–10769. <http://doi.org/10.1073/pnas.1834247100>
- Yu, L., Qi, M., Sheff, M. A., & Elion, E. A. (2008). Counteractive control of polarized morphogenesis during mating by mitogen-activated protein kinase Fus3 and G1 cyclin-dependent kinase. *Molecular Biology of the Cell*, 19(4), 1739–1752. <http://doi.org/10.1091/mbc.e07-08-0757>
- Yu, R. C., Pesce, C. G., Colman-Lerner, A., Lok, L., Pincus, D., Serra, E., ... Brent, R. (2008). Negative feedback that improves information transmission in yeast signalling. *Nature*, 456(7223), 755–761. <http://doi.org/10.1038/nature07513>
- Zeitlinger, J., Simon, I., Harbison, C., Hannett, N., Volkert, T. L., Fink, G., & Young, R. A. (2003). Program-specific distribution of a transcription factor dependent on partner transcription factor and MAPK signaling. *Cell*, 113(3), 395–404. [https://doi.org/10.1016/S0092-8674\(03\)00301-5](https://doi.org/10.1016/S0092-8674(03)00301-5)

SUPPORTING INFORMATION

Additional supporting information may be found online in the Supporting Information section at the end of the article.

How to cite this article: Shellhammer JP, Pomeroy AE, Li Y, et al. Quantitative analysis of the yeast pheromone pathway. *Yeast*. 2019;36:495–518. <https://doi.org/10.1002/yea.3395>